

Figure 1 (a) Momentum distribution of ^9Li fragments from the reaction ^{11}Li [800 MeV/nucleon] + C \rightarrow ^9Li + X. (b) Left: cracking a normal nucleus yields fragments with a momentum distribution well described by the Goldhaber formula. Right: cracking a halo nucleus requires a special treatment of the surface nucleons.

Break-up reactions and momentum distributions

1 Introduction

Fragmentation reactions with secondary beams of radioactive nuclei have shown that not only the reaction cross section but also the transverse momentum distribution of the fragments are sensitive to the separation energy of the last neutrons and to the size of the density profile in these nuclei [1]. These two quantities are linked since the “size” of the nucleus is roughly proportional to the inverse of the square root of the separation energy. Using the Goldhaber model for soft fragmentation, Tanihata and collaborators [1] were able to relate the widths of the narrow peaks in the transverse momentum distributions with the separation energies and sizes of the radioactive nuclei.

In Figure 1(a) we see the momentum distribution of ^9Li fragments from the reaction ^{11}Li [800 MeV/nucleon] + C \rightarrow ^9Li + X, taken from Ref. [2]. It is observed that to fit the experimental data one needs two Gaussian, or Lorentzian, functions. The broad peak is thought to involve nucleons which are *tightly bound*, while the narrow peak involves *valence*, weakly bound, nucleons.

2 Goldhaber model

A statistical model with minimal correlations was derived by Goldhaber [3] to explain the momentum distributions of projectile-fragments originating in peripheral collisions with heavy ions. In these experiments [4] it was observed that the momentum distributions of the fragments are well described by Gaussians, whose widths σ were found to follow a parabolic dependence on the mass of the fragment. In the statistical model this dependence is explained in terms of a single quantity, namely the rms momentum of the nucleons in the original projectile. Let us first recall the original Goldhaber derivation. In the statistical model the momentum of the fragment with mass number F is obtained by picking at random F nucleons from the projectile. In the frame of the projectile the average value (dispersion) of the square of the fragments momentum is given by

$$\sigma^2 = \left\langle \left[\sum_i^F \mathbf{p}_i \right]^2 \right\rangle = F \langle p_i^2 \rangle + F(F-1) \langle \mathbf{p}_i \cdot \mathbf{p}_j \rangle, \quad (1)$$

provided all come from a common distribution.

The second term in the above equation can be estimated in terms of $\langle p_i^2 \rangle$ by using the fact that the total momentum of the original nucleus is zero. This is in fact the only correlation used in the statistical model [3]. One obtains

$$\left\langle \left[\sum_i^A \mathbf{p}_i \right]^2 \right\rangle = A \langle p_i^2 \rangle + A(A-1) \langle \mathbf{p}_i \cdot \mathbf{p}_j \rangle = 0, \quad (2)$$

where $i \neq j$.

These two equations yield for the momentum dispersion of a fragment F the Goldhaber formula

$$\sigma^2 = \frac{F(A-F)}{(A-1)} \langle p_i^2 \rangle. \quad (3)$$

The quantity $\langle p_i^2 \rangle$ can be estimated by using shell-model wave functions, or the Fermi gas model for the nucleons. For a Fermi gas $\langle p_i^2 \rangle = 3p_F^2/5$. Generally, only one Cartesian component of the momentum distribution is measured. We then replace $\langle p_i^2 \rangle$ by $\sigma_0^2 = \langle p_i^2 \rangle / 3 = p_F^2/5$ [3].

In experiments with ^{11}Li projectiles, the narrow peak in the momentum distribution of ^9Li fragments has a width of $\sigma \sim 19$ MeV/c. This small momentum width reflects the weak binding energy of the last two neutrons in ^{11}Li . The wide peak with $\sigma \sim 95$ MeV/c, reflects the larger binding energy of the inner nucleons in ^{11}Li .

The simple and elegant derivation, due to Goldhaber, also displays nicely the parabolic dependence on the fragment mass F as observed in many experimental data [4]. From this derivation one sees that the averaging procedure does not make any extra assumption about nucleon-nucleon correlations, other than that the total momentum of the initial distribution is zero. Other kinds of correlations presumably

would affect the value of $\langle p_i^2 \rangle$, but not of $\langle \mathbf{p}_i \cdot \mathbf{p}_j \rangle$ when averaged over direction. However, Goldhaber's formula would not be well justified if, e.g. the spatial dependence of the fragmentation operator is so strong that a different treatment for nucleons at the nuclear surface and in the nuclear interior has to be considered separately [5]. In this regard we expect that the parallel momentum distributions are less sensitive to the fragmentation operator than the transverse distributions are. This is because transverse momentum distributions are more sensitive to the transverse geometry of the participating nuclei as well as to the Coulomb deflection of the projectile and fragments [7]. This was in fact observed experimentally [6]. When spatial dependence is relevant it is important to consider Pauli correlations among the nucleons in the statistical model [5], which would cause a reduction of the dispersion predicted by the Goldhaber model. We expect that other correlations, e.g., short-range correlations due to the nucleon-nucleon interaction, will also play an important role in such a case.

Supplement A

2.1 Extended Goldhaber model: a two-fluid statistical model

In general, the Goldhaber formula is quite successful, but some discrepancies with experiments have been observed in the past. For example, in some cases it has been observed that the momentum dispersion σ is about 30% smaller than predicted by the statistical model [8]. Experiments with radioactive nuclei have also shown some discrepancies with the statistical model [1, 9, 6, 10]. Experimentally it was also observed that the momentum distributions of neutrons are narrower by a factor of 2 than those for ${}^9\text{Li}$ fragments. The momentum distributions in such a weakly bound nucleus are presumably determined by their nuclear matter size [1]. However, while the momentum distribution of ${}^9\text{Li}$ suggests a halo size of 6-8 fm [6] in ${}^{11}\text{Li}$, the momentum distribution of neutrons seems to suggest a factor two larger. A possible explanation can be given with a statistical model for a system of two fluids of nucleons, as proposed by Bertulani and McVoy [11].

Let us now consider a nucleus composed of two "fluids" of nucleons with mass numbers A_1 and A_2 ($A = A_1 + A_2$). An alpha-particle inside a larger nucleus, or a ${}^9\text{Li}$ -core in ${}^{11}\text{Li}$, could be an example. Since the two fluids have to interact in order to keep the nucleus bound, one has to introduce another parameter K which is the relative momentum between the two fluids. Momentum conservation implies

$$\sum_i^{A_1} \mathbf{p}_i^{(1)} = \mathbf{K} = - \sum_j^{A_2} \mathbf{p}_j^{(2)}. \quad (4)$$

Using this relation we obtain

$$\langle \mathbf{p}_i^{(1)} \cdot \mathbf{p}_j^{(2)} \rangle = - \frac{\langle K^2 \rangle}{A_1 A_2} \quad \text{and} \quad \langle \mathbf{p}_i \cdot \mathbf{p}_j \rangle_N = \frac{\langle K^2 \rangle}{A_N (A_N - 1)} - \frac{\langle p^2 \rangle_N}{A_N - 1}, \quad i \neq j, \quad (5)$$

where $N = 1, 2$ and $\langle \rangle_N$ means average over nucleons in only one of the two fluids. The first equation is an average over nucleons in different fluids. We also express the nucleon momenta

with respect to the center of mass of their respective fluids. The relationship between their averages is

$$\langle p^2 \rangle_N = \langle \tilde{p}^2 \rangle_N + \langle K^2 \rangle / A_N^2 . \quad (6)$$

If we pick F nucleons from the projectile to make a fragment, the mean square momentum involves the cross-products given by the above equations. Assuming that the fragment can be composed of nucleons with equal probability from either of the two fluids, we can use Eq. 1 for the dispersion of the momentum distribution. In this case the quantities $\langle p_i^2 \rangle \equiv \langle p^2 \rangle$ and $\langle p_i \cdot p_j \rangle$ are to be averaged over the two distributions. One finds

$$\begin{aligned} \sigma^2 \equiv \left\langle \left[\sum_i^F \mathbf{p}_i \right]^2 \right\rangle &= F \left[\frac{A_1}{A} \langle p^2 \rangle_1 + \frac{A_2}{A} \langle p^2 \rangle_2 \right] \\ &+ F(F-1) \left[\frac{2A_1 A_2}{A(A-1)} \langle \mathbf{p} \cdot \mathbf{p}_j^{(2)} \rangle \right. \\ &+ \left. \frac{A_1(A_1-1)}{A(A-1)} \langle \mathbf{p}_i \cdot \mathbf{p}_j \rangle_1 + \frac{A_2(A_2-1)}{A(A-1)} \langle \mathbf{p}_i \cdot \mathbf{p}_j \rangle_2 \right] \\ &= \frac{F(A-F)}{A-1} \left[\frac{A_1}{A} \langle \tilde{p}^2 \rangle_1 + \frac{A_2}{A} \langle \tilde{p}^2 \rangle_2 + \frac{\langle K^2 \rangle}{A_1 A_2} \right] \quad (7) \end{aligned}$$

where the subindexes mean averages over the respective fluids. For $A_1 = A$ ($\langle K^2 \rangle = 0$) this equation reduces to Eq. 3.

Useful limits of Eq. 7 above can be obtained. E.g., when $\langle K^2 \rangle$ and $\langle \tilde{p}^2 \rangle_1 \ll \langle \tilde{p}^2 \rangle_2$ one gets (unless $A_1 \gg A_2$)

$$\sigma^2 \simeq \frac{A_2}{A} \frac{F(A-F)}{(A-1)} \langle \tilde{p}^2 \rangle_2 . \quad (8)$$

In such a situation we come to the important conclusion that the momentum dispersion of the fragments is reduced by a factor A_2/A relative to that obtained by means of Eq. 3.

In the fragmentation of ^{11}Li projectiles very narrow components were observed for the momentum distributions of ^9Li -fragments and of single neutrons [1, 9, 6, 10]. These widths (e.g., ~ 19 MeV/c for ^9Li -fragments [6]) cannot be explained by Eq. 8, unless an unrealistic value of the mean square momentum in ^9Li is assumed. To understand this we recall that Eqs. 7 and 8 are only adequate if enough energy is given to the projectile so that a fragment could be formed with nucleons from fluid A_1 or A_2 equally. But, in some situations [1] it has been observed that the energy transferred to the projectile is not enough to remove nucleons from the tightly-bound core, say fluid A_2 . The statistical average has to be carried out using a different procedure, as we explain next.

If one knows what fraction of nucleons in a given fragment come from one or the

other nuclear fluid then, instead of Eq. 7, one gets

$$\begin{aligned}
\sigma^2 &= F_1 \langle p^2 \rangle_1 + F_2 \langle p^2 \rangle_2 + F_1(F_1 - 1) \langle \mathbf{p}_i \cdot \mathbf{p}_j \rangle_1 \\
&+ F_2(F_2 - 1) \langle \mathbf{p}_i \cdot \mathbf{p}_j \rangle_2 + 2F_1F_2 \langle \mathbf{p}_i^{(1)} \cdot \mathbf{p}_j^{(2)} \rangle \\
&= \frac{F_1(A_1 - F_1)}{(A_1 - 1)} \langle \tilde{p}^2 \rangle_1 + \frac{F_2(A_2 - F_2)}{(A_2 - 1)} \langle \tilde{p}^2 \rangle_2 \\
&+ \left[\frac{F_1(F_1 - 1)}{A_1(A_1 - 1)} + \frac{F_2(F_2 - 1)}{A_2(A_2 - 1)} - \frac{2F_1F_2}{A_1A_2} \right. \\
&+ \left. \frac{F_1(A_1 - F_1)}{A_1^2(A_1 - 1)} + \frac{F_2(A_2 - F_2)}{A_2^2(A_2 - 1)} \langle K^2 \rangle \right]
\end{aligned} \tag{9}$$

where $F = F_1 + F_2$, and F_N comes from fluid N .

In the case of ${}^9\text{Li}$ fragments from ${}^{11}\text{Li}$ projectiles, one can identify the fragment as one of the constituent fluids of the nucleus, i.e., $F_1 = 0$, $F_2 = A_2$, and Eq. 9 becomes

$$\sigma^2 = \langle K^2 \rangle. \tag{10}$$

This is a trivial consequence of Eq. 4, if we use $F_2 = A_2$.

One observes that the nuclear potential holding the halo neutrons in ${}^{11}\text{Li}$ has a range not greater than 3 – 4 fm. However, due to their low binding energy these neutrons extend to a very large distance from the core, with an empirical rms radius for the halo matter distribution of about 6 fm [6]. Thus, the halo is a manifestation of a quantum tunnelling of the valence neutrons which extend to a region where their momenta are imaginary. Their wavefunctions in this region depend essentially on their binding energy. Therefore, it is more appropriate to equate $|\langle K^2 \rangle|$ with the separation energy $\langle B \rangle$ of the two-neutrons from the core. One finds

$$\langle B \rangle = \frac{2|\langle K^2 \rangle|}{m_N} \frac{A}{A_1A_2}. \tag{11}$$

Using the momentum width of 19 MeV/c for ${}^9\text{Li}$ fragments [6], one gets $\langle B \rangle = 0.44$ MeV, which is in fact very close to the separation energy of two neutrons in ${}^{11}\text{Li}$, i.e., $B = 0.34 \pm 0.05$ MeV.

As for the momentum width of a single halo neutron from ${}^{11}\text{Li}$, if in Eq. 9 we use $F_2 = 0$, $A_1 = 2$, $F_1 = 1$,

$$\sigma_n^2 = \frac{F_1(A_1 - F_1)}{(A_1 - 1)} \langle \tilde{p}^2 \rangle_1 + \frac{F_1^2}{A_1^2} \langle K^2 \rangle = \langle \tilde{p}^2 \rangle_1 + \frac{1}{4} \langle K^2 \rangle, \tag{12}$$

which is the momentum width in the laboratory (as it should be, according to Eq. 7. Since the radius of the halo is empirically about 6 fm, each neutron is confined within $\Delta x \simeq 12$ fm, so $\Delta p_x \geq \frac{1}{2}(\frac{1}{12 \text{ fm}}) = 8$ MeV/c. This is indeed in agreement with the measurements [10] and is about half the momentum width for the ${}^9\text{Li}$ fragment.

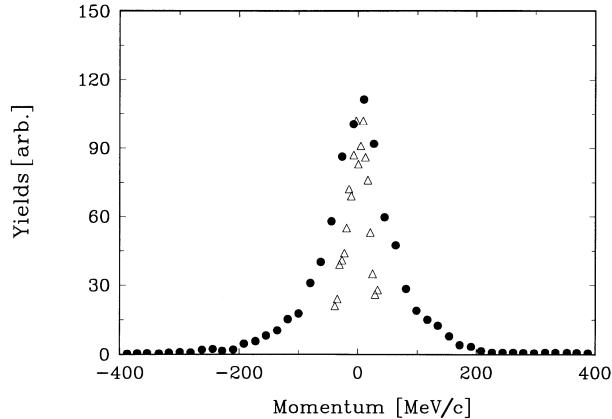


Figure 2 Comparison between the momentum distribution of ${}^9\text{Li}$ fragments from the reaction of ${}^{11}\text{Li}$ projectiles with Be (open triangles) [2] and C (closed circles) [6], at 70 MeV/nucleon and 800 MeV/nucleon, respectively.

3 Longitudinal \times transverse momentum distributions

A better measure of the interaction size of the radioactive projectile is obtained by the longitudinal momentum distribution of its fragments. Also, the Coulomb and nuclear fragmentation amplitudes have longitudinal momentum distributions with very nearly equal widths. This fact has indeed been verified in some experiments, see, e.g., [6]. On the other hand, the transverse momentum distributions are substantially broadened by the size and diffuseness of the region of overlap with the target and contain Coulomb and nuclear contributions with different widths. The interpretation of the “wide” (core-neutron) component of the transverse momentum distributions is therefore less straightforward than is for the longitudinal ones. Figure 2 shows the momentum distribution of ${}^9\text{Li}$ fragments from the reaction of ${}^{11}\text{Li}$ projectiles with Be (open triangles) [2] and C (closed circles) [6], at 70 MeV/nucleon and 800 MeV/nucleon, respectively. One clearly sees that the longitudinal momentum distributions are narrower than the transverse ones. There seems to be no need of a two-component fit of the experimental data in the first case. In other words, it seems that the longitudinal momentum distributions are a better way to study the momentum content of the nuclear halo, as shown in Ref. [7].

In what follows we will present a simple cluster description of the radioactive nuclei. That is we will assume that a single particle describes the halo, even in the case of ${}^{11}\text{Li}$ for which the two neutrons maybe assumed to form a di-neutron cluster. The conclusions drawn are however of general validity. The cluster model only serves as a guide to obtain a simpler insight into the results. The systems studied experimentally involve reactions of the form

$$a + A \rightarrow b + x + A^* \equiv b + X . \quad (13)$$

The starting point is a formula derived by Hussein and McVoy [12], but which

has a simple interpretation, as we discuss next. A spectator model of $a \equiv (b + x)$ gives the singles spectra of the particle b as

$$\frac{d\sigma}{d\Omega_b dE_b} = \rho(E_b) \frac{2E_x}{\hbar v_a k_x} \int d^2b_x |\tilde{\phi}_a(\mathbf{q}_b, \mathbf{b}_x)|^2 [1 - |S_{xA}(\mathbf{b}_x)|^2], \quad (14)$$

where

$$|\tilde{\phi}_a(\mathbf{q}_b, \mathbf{b}_x)|^2 = \left| \int d^3r_b e^{i\mathbf{q}_b \cdot \mathbf{r}_b} S_{bA}(\mathbf{b}_b) \phi_a(\mathbf{r}_b - \mathbf{r}_x) \right|^2. \quad (15)$$

If we do not know, or do not want to know, what happens to fragment x , we simply account for its absorption into X ($A + x$). This is taken care by the factor $[1 - |S_{xA}(b_x)|^2]$. (The quantity $S_{iA}(b_i)$ is the S-matrix for the scattering of cluster i ($i = b, x$) from the target A). But we also have to account for the transition probability for b to be removed from a (from the initial wavefunction $\phi_a(\mathbf{r}_b - \mathbf{r}_x)$) to the final free state $e^{i\mathbf{q}_b \cdot \mathbf{r}_b}$ (the distortion of this state by the interaction with the target is already included in $S_{bA}(\mathbf{b}_b)$). This is taken care by the overlap probability $|\tilde{\phi}_a(\mathbf{q}_b, \mathbf{b}_x)|^2$. The factors in front of the integral are from kinematic and phase-space considerations.

$S_{iA}(\mathbf{b}_i)$ can be obtained from a complex optical potential by means of the eikonal approximation. For the optical potential one can use the “ $t\rho\rho$ ” formalism, which is obtained by folding the nuclear densities of the participant nuclei weighted by the nucleon-nucleon scattering cross section, with medium correction effects. Bertulani and McVoy used this approach to study reactions involving ^{11}Li , ^{11}Be , and ^6He , and compare their results with the measurements of the momentum distributions of the ^9Li , ^{10}Be , and ^4He fragments, respectively. Thus in the cases of ^{11}Li and ^6He , we are assuming the two removed neutrons were assumed to behave in the projectile as a single cluster, which the collision removes as a unit. The Hartree-Fock densities for these nuclei were taken from Ref. [14], except for the ^6He , which was taken from Ref. [15]. The density distributions of the knocked-out neutrons were taken as the difference between the neutron distributions of the original nuclei and of the observed fragments.

In Eq. 15, ϕ_a represents the wavefunction for the incoming $a = (b + x)$ projectile. If one assumes that the fragment b does not interact with the target, i.e., $S_{bA}(\mathbf{b}) \equiv 1$, one finds

$$\frac{d\sigma}{d\Omega_b dE_b} = \rho(E_b) \sigma_{xA}^R |\phi_a(\mathbf{q}_b)|^2, \quad (16)$$

where σ_{xA}^R is the total reaction cross section of fragment x with the target A , and $\phi_a(\mathbf{q}_b)$ is the Fourier transform of $\phi_a(\mathbf{r}_b - \mathbf{r}_x)$ with respect to \mathbf{q}_b . The above result is known as the *Serber model limit* [16]. It tells us that in this approximation the breakup mechanism measures the momentum-space internal wavefunction of the projectile, so that the singles spectrum of fragment b provides important information about the internal structure of the projectile. This is especially useful for the study of extremely short-lived nuclei in secondary beam reactions.

Unfortunately, the Serber model is only a rough approximation for most cases and the elastic scattering (including absorption) of the fragment b on the target has

to be included, leading to an unavoidable broadening of the momentum distributions [17]. The physical origin of this broadening is simple diffraction (i.e., the uncertainty principle), as an examination of Eq. 15 makes clear. For instance, if $S_{bA} \equiv 1$, the Fourier transform given by this equation would be exactly the Fraunhofer diffraction pattern (as a function of \mathbf{q}_b) of the ‘‘source distribution’’ $\phi_a(\mathbf{r}_b - \mathbf{r}_x)$. Including the factor $S_{bA}(b_b)$, with $|S_{bA}(b_b)| \leq 1$, effectively decreases the transverse width of the source by eliminating the part that overlaps with the target A , and this will of course broaden the transverse diffraction pattern. A second possible source of transverse broadening is final-state Coulomb deflection, which is not included in Eq. 14.

This broadening makes it harder to extract the internal momentum structure of the projectile. However, since for high energy collisions the S-matrix S_{bA} does not depend on the longitudinal coordinate, the longitudinal momentum distribution is expected to be much less altered by the S_{bA} absorption. This can be illustrated by using a separable wavefunction, e.g. a Gaussian, in which case the longitudinal and transverse parts of the integral in Eq. (14) factorize completely. That is, if we take for the projectile cluster wave function the approximation $\phi_a \propto \exp\{-\mathbf{r}_b - \mathbf{r}_x\}^2 \Delta^2\}$ one finds

$$\begin{aligned} \frac{d\sigma}{dq_{//}^{(b)}} &= (2\pi)^2 \frac{E_x}{\hbar v_a k_x} \frac{C_\Delta^2}{\Delta^2} \exp\left\{-\frac{[q_{//}^{(b)}]^2}{2\Delta^2}\right\} \\ &\times \int d^2b_x b_x \exp\{-2\Delta^2 b_x^2\} [1 - |S_{xA}(b_x)|^2] \\ &\times \int db_b b_b \exp\{-2\Delta^2 b_b^2\} I_0(4b_x b_b \Delta^2) |S_{bA}(b_b)|^2, \end{aligned} \quad (17)$$

where the C_Δ is a normalization constant and I_0 a Bessel function. Thus, the dependence on $q_{//}^{(b)}$ is given by a Gaussian function multiplied by a geometrical factor. Therefore, the longitudinal momentum distribution measures the internal momentum function of the projectile and is insensitive to the details of the nuclear interaction. This result is exact for a Gaussian wavefunction, and is expected to be approximately true in general simply because S_{iA} is independent of the longitudinal coordinate.

Due to their low separation energies, the projectiles near the β -instability line are also easily Coulomb excited/fragmented [18]. For the moment we need some which will be justified *a posteriori*. The momentum distribution of the fragments will be determined by a matrix element of the form

$$\mathcal{M}_{if}^{(m)} = \int r Y_{1m}(\hat{\mathbf{r}}) \phi_f^*(\mathbf{r}) \phi_i(\mathbf{r}) d^3r. \quad (18)$$

The Coulomb fragmentation cross section is given in terms of this matrix element by [18]

$$\frac{d\sigma}{d\Omega_x d\Omega_b dE_b} = \frac{\mu_{bx}}{(2\pi)^3 \hbar^2} \frac{k_x k_b}{k_a} \sum_m |f_m(\mathbf{q}, \mathbf{Q})|^2, \quad (19)$$

where

$$f_m(\mathbf{q}, \mathbf{Q}) = \sqrt{\frac{16\pi}{3}} \frac{1}{2^{m/2}} \frac{Z_T e}{\hbar v} \left(\frac{k_a \omega}{v}\right) \chi_m(Q, q) \mathcal{M}_{if}^{(m)} \quad (20)$$

and

$$\chi_m(Q, q) = \int J_m(Qb) K_m\left(\frac{\omega b}{v}\right) S_{aA}(b) b db. \quad (21)$$

In the equations above $\mathbf{k}_a = \mathbf{k}_b + \mathbf{k}_x$, $\mathbf{q} = (m_x \mathbf{k}_b - m_b \mathbf{k}_x)/m_a$, $\mathbf{Q} = \mathbf{k}'_a - \mathbf{k}_a$ and $\hbar\omega = B + \hbar^2 q^2 / 2\mu_{bx}$, where B is the binding energy of the system $b + x$. To obtain the momentum distributions of fragment b we integrate the above equations with the constraint of energy conservation.

One can evaluate the Coulomb cross sections as well as the nuclear cross sections of Eq. 16 using an Yukawa wavefunction, $\phi \propto e^{-\eta r}/r$ for the initial cluster. For the final-state wavefunction one can use plane waves for the Coulomb breakup and Glauber for the nuclear breakup, as described in Ref. [12].

In the Figure 3 we show the longitudinal momentum distribution of ${}^9\text{Li}$ from the fragmentation of ${}^{11}\text{Li}$ projectiles with 70 MeV/nucleon. The data are from Ref. [6]. The data were taken using light and heavy targets, thus probing the relative strengths of the nuclear and the Coulomb interaction on the break-up. One can assume for simplicity that the momentum distributions for Be and Nb targets are induced by the nuclear interaction only, while for Ta targets the Coulomb interaction dominates. The distributions are then calculated by the separate use of Eqs. (14) and (19), respectively. The results are shown in Figure 3, together with the experimental data.

The calculations were repeated [11] using a Gaussian wavefunction and no significant difference in the distributions was found if the Gaussian parameter was chosen to be $\hbar\Delta = 20$ MeV/c.

We turn now to the investigation of the transverse momentum distributions. Figure 4 shows the transverse momentum distributions of ${}^9\text{Li}$, ${}^{10}\text{Be}$ and ${}^4\text{He}$ from the break-up of ${}^{11}\text{Li}$, ${}^{11}\text{Be}$ and ${}^6\text{He}$ projectiles, respectively, incident on carbon at 800 MeV/nucleon. For this target only the nuclear contribution to the break-up needs to be considered. The data are from Ref. [1]. The dotted curves are the result of the Serber model calculation following Eq. 16. The momentum parameters η of the Yukawa were taken as 27.8 MeV/c, 29 MeV/c and 49.2 MeV/c for ${}^{11}\text{Li}$, ${}^{11}\text{Be}$ and ${}^6\text{He}$, respectively, corresponding to binding energies of 0.25 MeV, 0.5 MeV and 0.97 MeV, respectively. The dashed curves were obtained using the more correct approach of Eq. 14, with the same values of η .

In the case of ${}^{11}\text{Li}$ the result of the Serber model agrees with the one obtained for the longitudinal momentum distribution data, since the momentum distribution given by this model is isotropic. The interaction of the fragments with the target broadens the peak, and this is displayed by the dashed curves in this figure. However, it is also seen that the wings of the momentum distributions cannot be reproduced by using a single Yukawa parameterization for the ground state wavefunction. This fact maybe due to the simple cluster model picture. More realistic models are able to describe these wings (wide component) [19], but the analysis is consistent with the idea that the narrow peak is closely related to the separation energy of the halo fragments.

An attempt to explain the wings of the momentum distributions displayed

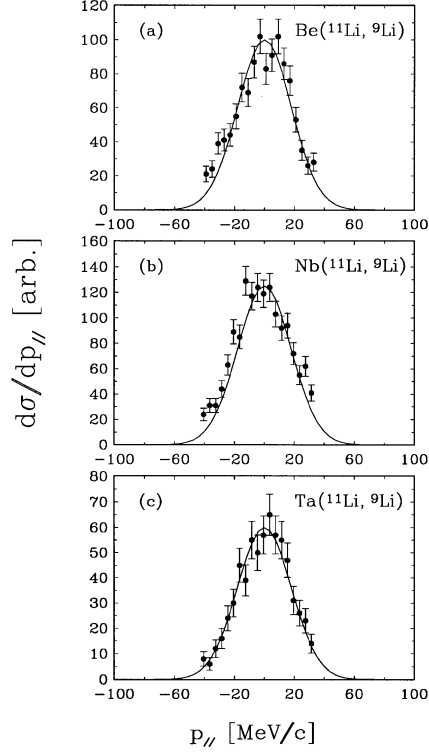


Figure 3 Longitudinal momentum distribution of ${}^9\text{Li}$ from the fragmentation of ${}^{11}\text{Li}$ projectiles with 70 MeV/nucleon. The data are from ref. [6].

in figure 4 (solid lines), can be made by assuming that also neutrons from the core of the projectile could be removed with appreciable probability [1]. One can assume that the cross sections for the removal of the loosely-bound valence neutrons and the more tightly-bound from the core add incoherently. The results are shown by the solid lines in figure 4. In this calculation one adds [11] two results of the Eq. (14), for simplicity using Gaussian wave functions $\phi \propto e^{-r^2/\Delta^2}$ for the core and halo neutrons. The values of $\hbar\Delta$ for the halo neutrons were taken as 19.5 MeV/c, 20.6 MeV/c and 34.7 MeV/c and those for the core neutrons as 55 MeV/c, 92 MeV/c and 79 MeV/c, for ${}^{11}\text{Li}$, ${}^{11}\text{Be}$ and ${}^6\text{He}$, respectively. They correspond to the approximate binding energies of valence and core nucleons, respectively. The Hartree-Fock densities for the core nucleons were taken from Ref. [14, 15]. The momentum widths of the “wings” are much wider than the ones cited earlier, and are related to the separation energies of the core neutrons. The contributions of the two Gaussian simulation for the internal wavefunctions were chosen so as to reproduce as well as possible the experimental data. The good agreement with the experimental data (solid lines in Fig. 4) should therefore be approached with some caution, since any two Gaussian fit can reproduce the transverse momentum data [1]. The ratio between the two

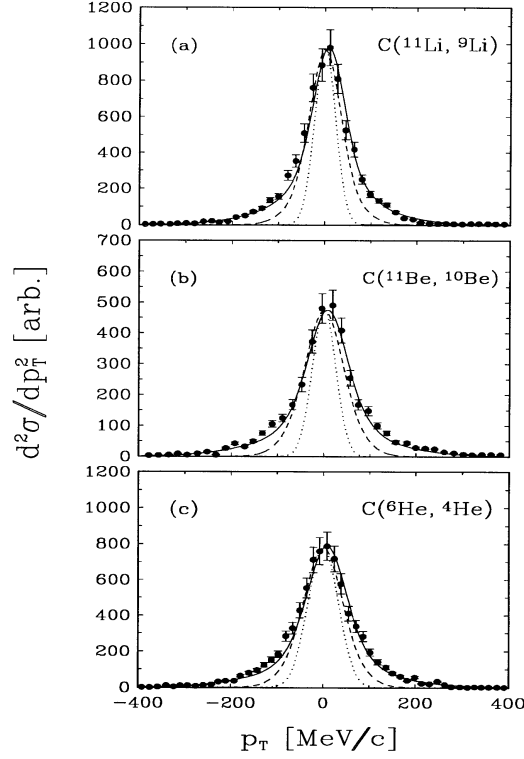


Figure 4 Transverse momentum distributions of ${}^9\text{Li}$, ${}^{10}\text{Be}$ and ${}^4\text{He}$ from the break-up of ${}^{11}\text{Li}$, ${}^{11}\text{Be}$ and ${}^6\text{He}$ projectiles, respectively, incident on carbon at 800 MeV/nucleon. The data are from ref. [1].

contributions presumably gives roughly the *spectroscopic factors* for the removal of neutrons from the core and from the halo, respectively.

Another interesting feature shown in Fig.4 is a small shift of the peaks with respect to the central position ($q_T = 0$). This shift arises from the phase of the S_i -matrices originating in the real part of the potential, but is small and may be neglected.

Supplement B

4 Ground state of a loosely-bound system

The Schrödinger equation for a system of two-particles can be reduced to an equation of the relative coordinates only (see Fig. 5(a)):

$$-\frac{\hbar^2}{2\mu}\nabla^2\psi(\mathbf{r}) + V(\mathbf{r})\psi(\mathbf{r}) = E\psi(\mathbf{r}) \quad (22)$$

where $\mu = m_1 m_2 / (m_1 + m_2)$.

For a spherically symmetric V , and $l = 0$ this equation reduces to

$$-\frac{\hbar^2}{2\mu} \frac{d^2 u}{dr^2} + V(r)u = Eu \quad (23)$$

where $\psi(\mathbf{r}) = u(r)/r$.

For simplicity lets us assume a square-well potential, i.e.,

$$V = \begin{cases} -V_0 & \text{for } r < r_0 \\ 0 & \text{for } r > r_0. \end{cases} \quad (24)$$

The solutions of 23 are

$$u(r) = \begin{cases} A \sin(kr), & r < r_0 \\ B e^{-\eta r}, & r > r_0 \end{cases} \quad (25)$$

with the constraint that u is finite at $r = \infty$. Matching the wavefunction and its derivative at $r = r_0$, yields the transcendental equation

$$k \cot k r_0 = -\eta \quad (26)$$

where

$$k = \sqrt{\frac{2\mu}{\hbar^2} (V_0 - B)} \quad ; \quad \eta = \sqrt{\frac{2\mu B}{\hbar^2}} \quad (27)$$

with $E = -B$ equal to the binding energy of the system.

The numerical solution of Eqs. 26 is given in Table 4.1, assuming $m_1 = m_2 = 938$ MeV and $B = 2.225$ MeV, corresponding to the deuteron.

r_0 (fm)	V_0 (MeV)
1	120
1.5	59
2	36
2.5	25
00	2.83

Table 4.1 - Range and depth of a square potential well which reproduces the binding energy of the deuteron.

For the deuteron $r_0 \sim 2$ fm, corresponding to $V_0 \sim 36$ MeV. But, the size of the deuteron is approximately given by $1/\eta \sim 4.3$ fm which is about twice that of the range of the potential (see Fig. 5(b)). Thus, the deuteron is a loosely-bound system. The nucleons spend much of their time in a region where their kinetic energy is imaginary (forbidden region), a phenomena known as quantum-tunneling.

When $V_0 \gg B$,

$$\cot(k r_0) = -\frac{\eta}{k} \cong -\sqrt{\frac{B}{V_0}} \quad (28)$$

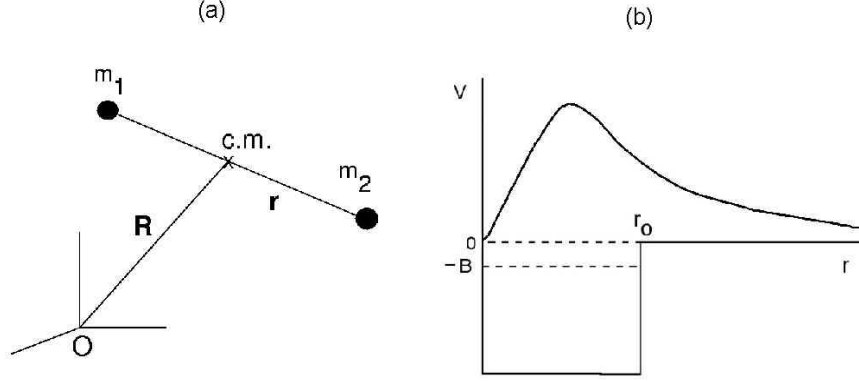


Figure 5 (a) Center of mass and relative coordinates of a two-body system. (b) Ground state wavefunction of the deuteron.

Thus, $\cos(kr_0) \cong 0$, or

$$kr_0 \cong \frac{\pi}{2}, \frac{3\pi}{2}, \dots \quad (29)$$

or

$$V_0 r_0^2 \cong \frac{\hbar}{m_N} \frac{\pi^2}{4}, \frac{\hbar^2}{m_N} \left(\frac{9\pi^2}{4} \right), \dots \quad (30)$$

Since u represents the ground-state, it cannot have a node. Thus, we only retain the 1st-term in 30. I.e., $V_0 r_0^2 \cong \pi^2 \hbar^2 / 4 m_N$.

5 Wounded wavefunction model

As we discussed in the previous Sections, the Serber mechanism seems to justify the assumption that the momentum distribution of a fragmentation product will be that of the initial wave function. In the following it will be shown that this does not hold in general, an argument due to P.G. Hansen [20]. The essential point is that collisions with a nuclear target cannot explore all parts of the halo's spatial wave function with equal probability, as we saw in Section ???. The momentum components transverse to the beam direction are known to carry the imprint of the reaction mechanism. For the parallel momentum components we have seen that they can be shown to be independent of the reaction mechanism for wave functions that factorize in cylindrical coordinates such as plane waves and Gaussians. However, the external two-body wave functions appropriate for halo states do not factorize, and the effect to be discussed arises from localization perpendicular to the beam direction.

Let us restrict ourselves here to purely nuclear reactions of single-nucleon halo systems with light targets. Good data exist for ^{11}Be [21] and ^8B [22], for which the structure is well understood [23, 24, 25] as predominantly an s-state halo neutron and a p-state halo proton, respectively. It is a good first approximation to represent these by a single-particle product wave function ψ_0 . The high projectile energies allow a

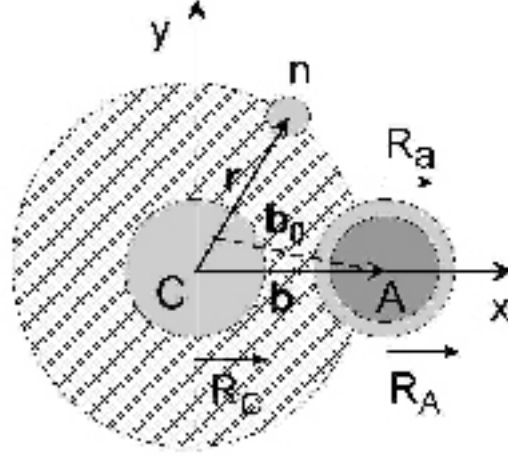


Figure 6 The coordinate system is centered in the projectile core C relative to which coordinate of the halo neutron is \mathbf{r} . The impact parameter of the target A (moving along the z -axis) is approximated by the two-dimensional vector \mathbf{b} instead of the vector \mathbf{b}_0 connecting to the center of mass. The target radii are the heavy-ion interaction radius R_A and the nucleon interaction radius R_a .

description in terms of a classical impact parameter b , see Fig. 6. The dissociation products ^{10}Be or ^7Be are formed at impact parameters greater than $b_{min} = R_C + R_A$, where the energy-dependent core and target radii are chosen to reproduce measured heavy-ion interaction cross sections [26]. There are two reaction channels: (i) nucleon stripping (or absorption) in which the halo nucleon has interacted strongly with the target and disappears from the beam, and (ii) diffraction dissociation in which the nucleon moves forward with essentially beam velocity (see Supplement C). Collisions at impact parameters smaller than b_{min} are assumed to lead to core fragmentation and hence will not contribute to the dissociation cross section.

The high beam energy also implies that the eikonal approximation is applicable. The target trajectory (in the coordinate system used here) is a straight line, and the range of the interaction, which does not have to be weak, is of the order of the effective target radius R_a . In this approximation (see Ref. [27]), the wave function of the halo state ψ_0 remains unchanged throughout all space except in a cylinder of radius R_a , where it is set to zero. This is the commonly used black-disk model. Its most important limitation, the assumption of a sharp target surface, is of little consequence in a discussion of the longitudinal momentum components.

Let the wave function originally contained in the reaction zone be denoted $\delta\psi_0$, a function that vanishes outside the interaction radius R_a , which can be chosen to reproduce the experimental reaction and elastic cross sections for free nucleons. Finally, the sudden approximation is valid. At the moment of impact, the nucleon stripping reaction selects the state of the system to be $\delta\psi_0$. The normalization P_a of this state is the stripping probability for a given b , and the square of its three-dimensional Fourier transform gives the momentum distribution, which must be that

of the core fragment since the halo nucleon is no longer present. For the same reason, the question of final-state interactions does not arise. If the nucleon is not stripped, the new state represented by the complement of the wave function $\psi_0 - \delta\psi_0$ is mainly the unchanged halo state. The (small) probability that it decays by diffraction dissociation is obtained directly if it is assumed [28] that the halo state ψ_0 is the only bound state of the system, which can be projected out to give the wave function of the decaying state $\psi_d = P_a \psi_0 - \delta\psi_0$ with normalization of $P_a^2 - P_a$. It will be seen that the first term in the wave function of the decaying state is a small correction, necessary to preserve orthogonality. Hence the probabilities of stripping and diffraction dissociation are approximately identical and equal to P_a . (This is related to the fact that the total cross section for fast neutrons is approximately twice the geometrical value.)

If final-state interactions are neglected, which seems to be a good approximation for ^{11}Be [28], the momentum distribution for diffraction dissociation is also given by the square of the Fourier transform of $\delta\psi_0$, which is then all that needs to be calculated. To obtain the probability distribution in momentum (written in terms of the wave vector \mathbf{k}) along the z axis for a general wave function $\psi(\mathbf{r})$, the square of its Fourier transform is integrated over k_x and k_y . This fivefold integral can be reduced to

$$\frac{dW}{dk_z} = \frac{1}{2\pi} \int \int \int \int \psi^*(x, y, z') \psi(x, y, z) \exp[ik_z(z - z')] dx dy dz dz' \quad (31)$$

a quantity that must now be evaluated with the wave function $\delta\psi_0$ introduced above. The differential cross section

$$\frac{d\sigma}{dk_z} = \int_{b_{\min}}^{\infty} \frac{dW}{dk_z} d\varphi b db \quad (32)$$

emerges as an integral over impact parameter.

For a narrow reaction zone with radius R_a it is a good approximation to replace the wave function in the integrand in 31 by its value $\delta\psi_0(b, 0, z)$ along the target trajectory. The integral over x and y now gives a factor πR_a^2 , which may be interpreted as the (free) nucleon reaction cross section. The contribution from diffraction dissociation relates in the same way to the elastic nucleon-target cross section. The sum of the two is obtained by replacing $2\pi R_a^2$ with the experimental [18] total cross section σ_T . If the integrand is symmetric about the z axis, Eq. 31 can be approximated as

$$\frac{dW}{dk_z} \simeq \frac{\sigma_T}{2\pi} |\exp(-ik_z z) \psi_0(b, 0, z) dz|^2 \quad (33)$$

since the two integrals over z and z' factorize. For initial states with l equal to 1 or greater, this expression must be averaged over initial m states in the usual way. It can easily be shown that, when taken in the limit of b_{\min} equal to zero, the integrals 33 followed by 32 give the true momentum distribution of the complete wave function, obtained more directly by substituting ψ_0 into Eq. 31. For the case of a halo neutron

with $l = 0, 1$, it is easy to derive closed expressions for Eqs. 32 and 32. As the reaction zone $\delta\psi_0$ is entirely outside the nuclear core, the exact external wave function is the first spherical Hankel function

$$\delta\psi_0(\mathbf{r}) = Bk^{3/2}h^l(i\eta r)Y_{lm}(\theta, \phi) \quad (34)$$

written in terms of the reduced mass and neutron separation energy through the relation $\eta = (2\mu S_n)^{1/2}/\hbar$. The dimensionless constant B , of order unity, is determined by joining the outer and inner solutions to the Schrödinger equation. For an $l = 0$ state, a Yukawa wave function corresponds to the choice $B = \sqrt{2}$ (sometimes [28] augmented by a finite-size correction), while a Woods-Saxon calculation suggests $B = 2.26$ for ^{11}Be . For a p state and a neutron binding energy of 0.137 MeV (corresponding to that of the proton in ^8B), one has $B = 0.47$. The integral 33 for $l = 0$ is given in sect. 3.961 of [29],

$$\frac{dW_l}{dk_z} = \frac{\sigma_T B^2 \eta}{2\pi^2} K_0^2(\chi) , \quad (35)$$

and partial differentiation of the two integrals given in the same reference with respect to the impact parameter b leads to the expression for $l = 1$,

$$\frac{dW_l}{dk_z} = \frac{\sigma_T B^2}{2\pi^2 \eta} [k_z^2 K_0^2(\chi) + (k_z^2 + \eta^2) K_1^2(\chi)] , \quad (36)$$

where the argument of the modified Bessel functions is $\chi = b(k_z^2 + \eta^2)^{1/2}$. The two terms inside the square bracket in Eq. 36 are the contributions from the $m = 0$ and $m = \pm 1$, respectively, the latter being the most important. The differential cross sections can now be obtained by integrating Eqs. 35 and 36 over b to give for $l = 0$

$$\frac{d\sigma_0}{dk_z} = \frac{\sigma_T B^2 \eta b_{\min}}{2\pi} [K_1^2 - K_0^2] , \quad (37)$$

and for $l = 1$

$$\frac{d\sigma_1}{dk_z} = \frac{\sigma_T B^2 b_{\min}}{2\pi \eta} \left[k_z^2 (K_1^2 - K_0^2) + (k_z^2 + \eta^2) \left(K_1^2 - K_0^2 - \frac{2}{\xi} K_0 K_1 \right) \right] , \quad (38)$$

where the argument of the modified Bessel (McDonald) functions is understood to be $\xi = b_{\min}(k_z^2 + \eta^2)^{1/2}$. The single-nucleon stripping cross sections are obtained by integrating over k_z . Results obtained with Eqs. 35-38 are shown in Figs. 7 and 8.

Complete single-particle wave functions were calculated in a Woods-Saxon potential-well model with radius and diffuseness parameters $r_0 = 1.25$ fm ($R = r_0 A^{1/3}$ fm) and $a = 0.7$ fm and with the well depth adjusted to reproduce the experimental separation energy. The results obtained for neutrons when Eqs. 32 and 33 were evaluated numerically with these wave functions were identical with the results of Eqs. 35-38 to within 1% as could be expected since, in this case, Eq. 34 is an exact solution outside the range of the potential. For the ^8B calculations, Fig. 33, the

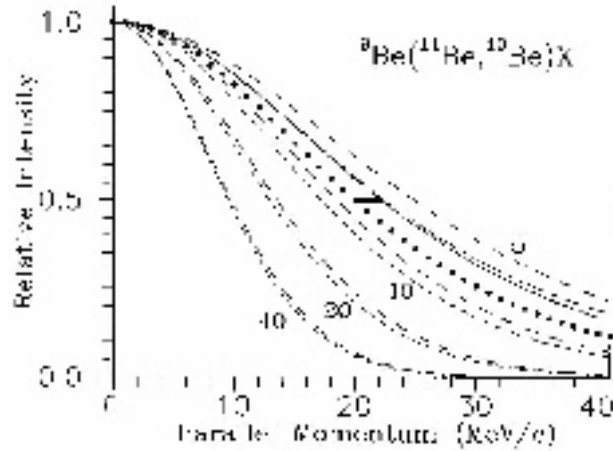


Figure 7 Calculations for the ^{11}Be s -state halo incident on a beryllium target and for a beam energy of 63 MeV/u. (i) All parallel momentum distributions are normalized to unity at the origin; the bar is the measured half width at half maximum, and the large dots represent the differential cross section $d\sigma/dp_z$. The full-drawn line is the distribution dW/dp_z of the total wave function. (ii) The four pairs of dashed curves correspond to the quantity dW/dp_z for fixed impact parameters of 5, 10, 20, and 40 fm with the long and short dashes denoting the respective limits of small target radius (eq. 35) and infinite target radius (planar cutoff).

Coulomb potential acting on the halo proton was taken as that of a uniformly charged sphere with the same radius as the Woods-Saxon well. The results are insensitive to the choice of the Coulomb radius. The approximation leading to Eq. 33 assumes that the effective radius R_a of the target is small. (At 63 MeV/u it is of the order of 2.0 fm for ^9Be as compared with a decay length of the ^{11}Be halo wave function of 6.75 fm.) This assumption can be tested in the other extreme limit, that of infinite target radius, in which the reaction zone is bounded by a planar cutoff. Expressions for this case have been given in Ref. [30]. The four pairs of dashed curves shown in Fig. 7 demonstrate that the two extreme approximations give nearly identical results, and also that the parallel-momentum distributions depend strongly on the impact parameter. The momentum distributions of the cross section are shown as large dots in Figs. 7 and 8, and the widths and dissociation cross sections are in good agreement [20] with the experimental results [21, 22, 28, 32]. The cross sections, roughly one-third and one-tenth of the free-nucleon values, provide a valuable quantitative verification of the simple model used. It is seen that the calculation, in agreement with that of Ref. [33], satisfactorily explains the reduction of ^8B width to roughly half of that of the total wave function, 153 MeV/c. This apparent discrepancy had originally led to the claim [22] that an interpretation in terms of a complex many-particle wave function was required. As the effect of localization must in any case be present, it should not be viewed as a possible alternative explanation. Two curves in Fig. 8 demonstrate that a p -state neutron would behave similarly.

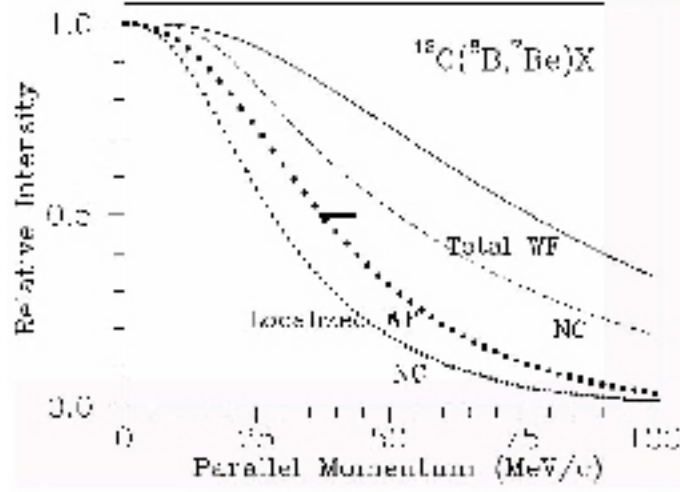


Figure 8 Calculations for the ${}^8\text{B}$ p -state halo incident on a carbon target and for a beam energy of 1471 MeV/u. The notation is the same as for fig. 7 (i). It is seen that the localization effect reduces the width by a factor of 2, in agreement with experiment. The other pair of curves, dashed and small dots, are calculated for no Coulomb (NC) interaction in the halo state. The localization effect is, in this case, given by eq. 38 and illustrates the case of a hypothetical p -state neutron with otherwise unchanged parameters.

The interpretation given here has an important implication for the analysis of experimental data. The longitudinal momentum distributions measured with a light target should, to lowest order, not be affected by the transverse acceptance of the spectrometer. In the approximation leading to Eq. 35 the radial momentum distribution becomes proportional to $[J_1(k_r R_a)/k_r R_a]^2$, the usual diffraction pattern (see Supplement C), depending only on the radius of the target. Clearly, all information about the original momentum in the x - y plane has been destroyed by the measurement. The corresponding radial broadening has been detected [30, 28] for neutrons. This means that the wave function at the moment of the collision takes a form that factorizes (see earlier comments), and the k_z distribution will not be changed by an incomplete detection of the k_x and k_y components.

Supplement C

5.1 Diffraction dissociation

The amplitude for the dissociation of a cluster projectile incident on a target nucleus, assumed to stay in its ground state, is given in the eikonal approximation by

$$f_d(\mathbf{q}, \mathbf{Q}) = \frac{ik}{2\pi} \int d^2b e^{i\mathbf{Q}\cdot\mathbf{b}} \Gamma_d(\mathbf{b}) , \quad (39)$$

where \mathbf{k} is the center of mass momentum of the projectile, \mathbf{Q} is the momentum change in the scattering ($Q = 2k \sin(\theta/2) \simeq k\theta$, where θ is the scattering angle in the center of mass), \mathbf{q} is the relative motion momentum of the outgoing fragments, and \mathbf{k}_1 and \mathbf{k}_2 are the momenta of the corresponding clusters with masses m_1 and m_2 , respectively. In non-relativistic collisions $\mathbf{q} = (m_2\mathbf{k}_1 - m_1\mathbf{k}_2) / (m_1 + m_2)$ while for high-energetic collisions \mathbf{q} can be determined by the invariant mass of the two fragments. $\Gamma_d(\mathbf{b})$ is the profile function for the dissociation. For processes dominated by nuclear scattering, and assuming a sharp boundary target, it can be written as $\Gamma_d(\mathbf{b}) = \Gamma_N(\mathbf{b})$, where $\Gamma_N(\mathbf{b})$ vanishes for $b > R$.

The total dissociation cross section is given by

$$d\sigma = \left| f_d(\mathbf{q}, \mathbf{Q}) \right|^2 d\Omega d^3q / (2\pi)^3, \quad (40)$$

where

$$d\Omega \simeq (2\pi/k^2) Q dQ \quad (41)$$

for high-energy collisions.

According to Eq. 25, the relative motion of the clusters within the projectile is described by the wave function

$$\psi_i = \sqrt{\eta/2\pi} e^{-\eta r} / r, \quad (42)$$

where $\eta = \sqrt{2\mu\epsilon/\hbar^2}$ is determined by the separation energy ϵ of the clusters (1+2) and μ is the reduced mass of the system (1+2). The relative motion of the clusters released after the disintegration of projectile is described by the wavefunction

$$\psi_i(r) = e^{i\mathbf{q}\cdot\mathbf{r}} + \frac{1}{iq - \eta} \frac{e^{-iqr}}{r}. \quad (43)$$

These wavefunctions correspond to the assumption of zero-range nuclear forces between the clusters in the projectile. They are very useful because most of the following calculations can be performed analytically. An extension to the use of more realistic wavefunctions is straight-forward. They form a complete set of orthogonal functions satisfying the relation

$$\psi_i(\mathbf{r}) \psi_i^*(\mathbf{r}') + \frac{1}{(2\pi)^3} \int \psi_f(\mathbf{r}) \psi_f^*(\mathbf{r}') d^3q = \delta(\mathbf{r} - \mathbf{r}'). \quad (44)$$

The use of the above wavefunctions presupposes a simple model, where the Coulomb repulsion between the clusters are not taken into account. The Coulomb repulsion between the clusters must lose its importance for high relative motion after their dissociation. By using the energy and momentum conservation laws, we can also express Eq. 40 in terms of coincidence cross sections which are of interest in inclusive experiments. One finds

$$\frac{d^3\sigma}{d\Omega_1 d\Omega_2 dE_2} = \frac{\mu}{(2\pi)^3 \hbar^2} \frac{k_1 k_2}{k} |f_d(\mathbf{q}, \mathbf{Q})|^2, \quad (45)$$

where Ω_1 and Ω_2 are the solid angles of emission of the two fragments, and E_2 is the energy of one of them.

The amplitudes for diffraction dissociation of deuterons by a black nucleus were calculated in Ref. [34]. The extension to the dissociation of other weakly bound nuclei [18] gives

$$f_N(\mathbf{q}, \mathbf{Q}) = ikR \left\{ \frac{J_1(QR)}{Q} [F(-\beta_2 \mathbf{Q}, q) + F(\beta_1 \mathbf{Q}, q)] - \frac{ikR^2}{2\pi} \int d^2Q' \frac{J_1(Q'R)}{Q'} \frac{J_1(|\mathbf{Q} - \mathbf{Q}'|R)}{|\mathbf{Q} - \mathbf{Q}'|} F(\beta_1 \mathbf{Q} - \mathbf{Q}', q) \right\}, \quad (46)$$

where $\beta_2 = m_2/(m_1 + m_2)$, $\beta_1 = m_1/(m_1 + m_2)$, $R = 1.2A_T^{1/3}$ fm is the radius of the target nucleus, and

$$\begin{aligned} F(\mathbf{Q}, \mathbf{q}) &= \int d^3r \psi_f^*(\mathbf{r}) e^{i\mathbf{Q}\cdot\mathbf{r}} \psi_i(\mathbf{r}) \\ &= \sqrt{8\pi\eta} \left\{ \frac{1}{\eta^2 + (\mathbf{Q} - \mathbf{q})^2} + \frac{1}{2Q(i\eta - q)} \ln \left[\frac{q + Q + i\eta}{q - Q + i\eta} \right] \right\}. \end{aligned} \quad (47)$$

The first term in Eq. 46 corresponds to the impulse approximation, i.e., the independent scattering of separate clusters by the target. The second term corresponds to the simultaneous scattering of the clusters, also called by ‘‘eclipse’’, or ‘‘shadowing’’, term. In order to describe the differential cross sections, we can use only the impulse approximation, which gives reasonable results for small scattering angles. But, in order to obtain the total diffraction cross sections we have to include the shadowing term, since it decreases more slowly with increasing Q , and becomes the dominant contribution to the scattering amplitude (46) for larger values of Q .

Inserting 46 into Eq. 40 and using the orthonormality conditions of the wavefunctions, the integration over q can be easily performed in the impulse approximation. One gets

$$\begin{aligned} \frac{d\sigma}{dQ} &= \frac{2\pi R^2}{Q} J_1^2(QR) \left\{ \int d^3r |\psi_i(\mathbf{r})|^2 \left| e^{i\beta_1 \mathbf{Q}\cdot\mathbf{r}} + e^{-i\beta_2 \mathbf{Q}\cdot\mathbf{r}} \right|^2 \right. \\ &\quad \left. - \left| \int d^3r |\psi_i(\mathbf{r})|^2 \left[e^{i\beta_1 \mathbf{Q}\cdot\mathbf{r}} + e^{-i\beta_2 \mathbf{Q}\cdot\mathbf{r}} \right] \right|^2 \right\}, \end{aligned} \quad (48)$$

which gives

$$\begin{aligned} \frac{d\sigma}{dQ} &= \frac{2\pi R^2}{Q} J_1^2(QR) \left\{ 1 + \frac{2\eta}{Q} \arctan\left(\frac{q}{2\eta}\right) \right. \\ &\quad \left. - \frac{2\eta^2}{Q^2} \left[\frac{1}{\beta_1} \arctan\left(\frac{\beta_1 Q}{2\eta}\right) + \frac{1}{\beta_2} \arctan\left(\frac{\beta_2 Q}{2\eta}\right) \right] \right\} \end{aligned} \quad (49)$$

Using Eq. 49 we find that for $\eta \rightarrow \infty$, corresponding to infinite binding energy of the clusters, $d\sigma_N/dQ \rightarrow 0$. For $\eta \rightarrow 0$, corresponding to very loosely bound nuclei,

$$\frac{d\sigma}{dQ} \rightarrow \frac{4\pi R^2}{Q} J_1^2(QR), \quad (50)$$

which means that in this case the total nuclear dissociation cross section will be just the sum of the elastic diffraction cross section for each cluster separately. Both limits is what one expects from the simple arguments of the diffraction dissociation method. But, for large values of Q the impulse approximation is not more reasonable: the second term of Eq. 40 will increase in importance for $Q \gtrsim \eta$. Therefore, to obtain the contribution of the diffraction dissociation to the total dissociation cross section, one has to integrate 40 numerically, using 46 and 47.

6 Elastic and inelastic break-up of halo nuclei

One of the major differences between exotic neutron-rich or proton-rich nuclei and normal nuclei is the larger probability in the former of breaking up owing to the smaller binding energy of the halo cluster. This results in two different processes: the elastic breakup of the projectile which leaves the target intact in its ground state with the two (or more) fragments flying apart, and the inelastic breakup, when one of the fragments interact strongly with the target while the other, usually the observed one, passes by only feeling the optical distortion of the target. The former is also called “*diffractive breakup*” while the latter “*stripping*”. Here we shall use the previous names: *elastic breakup* and *inelastic breakup*. There are in principle other processes which may contribute, especially at lower energies, such as the gradual loss of energy of the projectile in the entrance channel before the breakup occurs.

An important feature of inelastic breakup is its potential use to extract spectroscopy information of the orbital form which the interacting fragment has originated. All the models of elastic and inelastic breakup rely on the use of the Glauber models [35, 36, 37, 38, 39, 40] or a time dependent variance of it developed by Bonaccorso and Brink [41, 42, 43]. In the next Sections we shall present first the Glauber theory for elastic and inelastic breakup and supply a reaction theoretical foundation for it which was earlier derived by Hussein and McVoy (HM) [12]. We should mention that most of the theoretical development in this area were done in the 70’s and 80’s for deuteron break up [44, 45, 59, 46].

The reaction we desire to describe is

$$a + A = (b + c) + A \rightarrow c + b + A \rightarrow c + (b + A) \rightarrow b + (c + A) \quad (51)$$

where the projectile a is considered to be formed by a core, c , and a halo particle, b . In cases of two-neutron halo, b should be considered on composed of two neutrons: the dynamics becomes more complicated as sequential processes may occur in general (both for *Borromean* as well as *non-Borromean* halo nuclei).

In the eikonal approximation, the phase shift is linear in the interaction. Then, according to Glauber, the scattering of a composite object from a structure particle (since we consider events where the target is presumed to remain in the ground state), the S-matrix for $a + A$ can be written as

$$\widehat{S}_a = \widehat{S}_b \widehat{S}_c \quad (52)$$

where the \widehat{S} is still an operator since it refers to a particle inside the projectile and this depends on parameters that have to be averaged over by the ground state wave function of projectile, ϕ_0 . The elastic breakup cross section can be easily calculated (the observed particle is c)

$$\sigma_{el.bup} = \sum_{\mathbf{k}} \left| \langle \phi_{\mathbf{k}} | \widehat{S}_b \widehat{S}_c | \phi_0 \rangle \right|^2 \quad (53)$$

where $\phi_{\mathbf{k}}$ is wave function that represents the continuum of b and c . Since $\int |\phi_{\mathbf{k}} \rangle \langle \phi_{\mathbf{k}}| d\mathbf{k} + |\phi_0 \rangle \langle \phi_0| = 1$, the above expression can be simplified

$$\begin{aligned} \sigma_{el.bup} &= \int \langle \phi_0 | \widehat{S}_b^* \widehat{S}_c^* | \phi_{\mathbf{k}} \rangle \langle \phi_{\mathbf{k}} | \widehat{S}_b \widehat{S}_c | \phi_0 \rangle d\mathbf{k} \\ &= \langle \phi_0 | |\widehat{S}_b|^2 |\widehat{S}_c|^2 | \phi_0 \rangle - \left| \langle \phi_0 | \widehat{S}_b \widehat{S}_c | \phi_0 \rangle \right|^2 \end{aligned} \quad (54)$$

The above expression has been used by several authors to obtain the elastic breakup contribution to the cross-section, as we have shown in previous Sections.

In so far as the inelastic break up is concerned, one realizes that the detected particle must reach the detector intact and thus one must use a survival probability to guarantee this. This survival probability is $|\widehat{S}_c|^2$. On the other hand the interacting fragment b is removed (stripped) and the probability for this to happen is $\left(1 - |\widehat{S}_b|^2\right)$. Identifying the transmission coefficient T_b with $1 - |\widehat{S}_b|^2$, we can write for the inelastic break up the following expression

$$\sigma_{in.bup} = \frac{\pi}{k_a^2} \sum \langle \phi_0 | \left(1 - \widehat{T}_c\right) \widehat{T}_b | \phi_0 \rangle \quad (55)$$

The above cross-section is also called the b removal cross-section with the notation σ_{-b} . Of course one may have the removal of the core (less probable owing to the Coulomb barrier between the charged core and the target)

$$\sigma_{-c} = \frac{\pi}{k_a^2} \sum \langle \phi_0 | \left(1 - \widehat{T}_b\right) \widehat{T}_c | \phi_0 \rangle \quad (56)$$

the sum of σ_{-b} and σ_{-c} gives

$$\sigma_{-b} + \sigma_{-c} = \frac{\pi}{k^2} \sum \langle \phi_0 | \widehat{T}_c + \widehat{T}_b - 2\widehat{T}_b \widehat{T}_c | \phi_0 \rangle \quad (57)$$

summing the above with the *total fusion* of a , described here by $\sigma_{-a} \equiv \sigma_{fusion} = (\pi/k^2) \sum \langle \phi_0 | \widehat{T}_b \widehat{T}_c | \phi_0 \rangle$, gives

$$\begin{aligned} \sigma_{-b} + \sigma_{-c} \sigma_{-a} &= \frac{\pi}{k^2} \sum \langle \phi_0 | \widehat{T}_c + \widehat{T}_b - \widehat{T}_b \widehat{T}_c | \phi_0 \rangle \\ &= \frac{\pi}{k^2} \sum \langle \phi_0 | \left(1 - |S_b|^2 |S_v|^2\right) | \phi_0 \rangle = \sigma_{reaction}, \end{aligned} \quad (58)$$

which confirms unitarity.

The expressions for $\sigma_{el.bup}$, Eq. 54, and $\sigma_{in.bup}$, Eq. 55, have been used by several authors to analyze the data on halo nuclei. It has been common to call $\sigma_{el.bup}$, the *diffractive break-up* cross section and $\sigma_{in.up}$ the *stripping* cross section [35, 36, 37, 38, 39, 40].

Supplement D

7 Reaction theory of elastic and inelastic break-up

In this Supplement we give a formal reaction theory background for the discussion in the previous section. We rely on the work of Austern et al [44], and Hussein & McVoy [12].

The full Schrödinger equation that describes the reaction in 51, can be obtained from the Hamiltonian:

$$H = (H_b + H_c + H_A + V_{bc} + V_{cA} + V_{bA} + K_b + K_c + K_A), \quad (59)$$

where H_i is the intrinsic Hamiltonian of nucleon i , V_{ij} is the full interaction (real) between i and j and K_i is the kinetic energy operator.

We shall now make several approximations:

$$H |\Xi\rangle = E |\Xi\rangle \quad (60)$$

i) $H_A = 0$ (heavy target);

ii) $V_{cA} = U_c$, the complex optical potential of the core: the spectator model;

iii) $H_b = H_c = 0$, both core and participating particle are structureless.

Now we calculate the inclusive break-up cross-section (elastic + inelastic break up).

The detected particle is the core c ,

$$\frac{d^2\sigma}{d\Omega_c dE_c} = \frac{2\pi}{\hbar v_a} \rho(E_c) \sum_i \left| \left\langle \chi_c^{(-)} \Psi_{bA}^{(i)} | V_{cb} | \Xi^{(+)} \right\rangle \right|^2 \delta(E - E_c - E_i) \quad (61)$$

In the above $\Psi_{bA}^{(i)}$ is the exact wave function of the $b + A$ system

$$(E^i - H_A - K_b - V_{bA}) \Psi_{bA}^{(i)} = 0 \quad (62)$$

and $\chi_c^{(-)}$ is the distorted wave of the observed particle

$$(E_c - K_c - U_c) \left| \chi_c^{(-)} \right\rangle = 0 \quad (63)$$

Note that V_{bA} is a fully microscopic interaction, $\sum_{k=1}^A V_{bk}$, where V_{bk} is the real interaction of b (structureless with nucleon k in the target). Finally $\rho(E_c)$ is the appropriate momentum phase-space density of the observed particle (core)

$$\rho(E_c) = \frac{\mu_c k_c}{(2\pi)^3 \hbar^2}. \quad (64)$$

Notice that the sum over i is a short hand notation for the sum of all unobserved momenta and states.

Since the argument of the delta function contains E^i , the eigen-value of the Schrödinger Eq. for $\Psi_{bA}^{(i)}$, Eq. 62, we can replace the delta function by an operator

$$\begin{aligned} & \left| \Psi_{bA}^{(i)} \right\rangle \delta(E - E_c - E^i) \left\langle \Psi_{bA}^{(i)} \right| = \left| \Psi_{bA}^{(i)} \right\rangle \delta(E - E_o - H_A - K_b - V_{bA}) \left\langle \Psi_{bA}^{(i)} \right| \\ & = \frac{1}{\pi} \text{Im} \left| \Psi_{bA}^{(i)} \right\rangle \frac{1}{E - E_c - H_A - K_b - B_{bA} + i\varepsilon} \left\langle \Psi_{bA}^{(i)} \right| = \frac{1}{\pi} \text{Im} \left| \Psi_{bA}^{(i)} \right\rangle G_{bA}^{(+)} \left\langle \Psi_{bA}^{(i)} \right| \end{aligned} \quad (65)$$

where $G_{bA}^{(+)}$ is the many-body Green's function of the $b + A$ system. With the above the cross-section can be written as

$$\frac{d^2\sigma}{d\Omega_c dE_c} = \frac{2}{\hbar v_a} \rho(E_c) \text{Im} \sum_i \left\langle \Xi | V_{cb} | \chi_c^{(-)} \Psi_{bA}^i \right\rangle G_{bA}^{(+)} \left\langle \chi_c^{(-)} \Psi_{bA}^{(+)} | V_{cb} | \Xi \right\rangle \quad (66)$$

The sum over the complete set Ψ_{bA}^i can now be performed (closure) to obtain

$$\frac{d^2\sigma}{d\Omega_c dE_c} = \frac{2}{\hbar v_a} \rho(E_c) \text{Im} \left[\left\langle \Xi | V_{cb} | \chi_c^{(-)} \right\rangle G_{bA}^{(+)} \left\langle \chi_c^{(-)} | V_{cb} | \Xi \right\rangle \right] \quad (67)$$

The cross-section becomes

$$\frac{d^2\sigma}{d\Omega_c dE_c} = \frac{2}{\hbar v_a} \rho(E_c) \left[\left\langle \Psi_0 | V_{cb} | \chi_c^{(-)} \right\rangle \left(\text{Im} G_b^{(+)} \right) \left\langle \chi_c^{(-)} | V_{cb} | \Psi_0 \right\rangle \right] \quad (68)$$

The above expression is an exact three-body form for the inclusive singles spectrum of particle c which contains both elastic and inelastic break up. It is convenient to separate these two components. For this purpose we use the following expression for $\text{Im} G_b^{(+)}$

$$\text{Im} G_b^{(+)} = \pi \int \frac{d\mathbf{k}_b}{(2\pi)^3} \left| \chi_b^{(-)} \right\rangle \left\langle \chi_b^{(-)} \right| \left[\delta(E - E_c - E_b) - G_b^{(+)\dagger} (-W_b) G_b^{(+)} \right] \quad (69)$$

where $-W_b$ is the imaginary part of U_b and represents the loss of the b flux owing to its interaction with the target.

Thus

$$\frac{d^2\sigma}{d\Omega_c dE_c} = \frac{d^2\sigma_{el.bup}}{d\Omega_c dE_c} + \frac{d^2\sigma_{ine.bup}}{d\Omega_c dE_c}, \quad (70)$$

where

$$\frac{d^2\sigma_{el.bup}}{d\Omega_c dE_c} = \frac{2\pi\rho(E_c)}{\hbar v_a} \int \frac{d\mathbf{k}_b}{(2\pi)^3} \left| \left\langle \chi_b^{(-)} \chi_c^{(-)} | V_{xb} | \Psi_0^{(+)} \right\rangle \right|^2 \delta(E - E_c - E_b - \varepsilon_0) \quad (71)$$

and

$$\frac{d^2\sigma_{ine.bup}}{d\Omega_c dE_c} = \frac{-2\rho(E_c)}{\hbar v_a} \int \left\langle \Psi_0 | V_{cb} G_b^{(+)\dagger} | \chi_c^{(-)} \right\rangle W_b(\mathbf{r}_b) \left\langle \chi_c^{(-)} | G_b^{(+)} V_{cb} | \Psi_0 \right\rangle d\mathbf{r}_b \quad (72)$$

Now

$$(E - U_b - U_c - V_{bc} - K_b - K_c) \Psi_0 = 0 \quad (73)$$

Thus

$$\begin{aligned} \Psi_0 V_{bc} &= \Psi_0 (E - U_b - U_c - K_b - K_c) \\ \langle \Psi_0 | V_{cb} G_b^\dagger | \chi_c^{(-)} \rangle &= \langle \Psi_0 | (E - K_c - U_c^\dagger - K_b - U_c^\dagger) \\ G_b^{(+)\dagger} (U_c + K_c) \chi_c^{(-)} &= \langle \Psi_0 | \chi_c^{(-)} \rangle \end{aligned} \quad (74)$$

Thus, we obtain the three-body expression of the inelastic break up cross-section

$$\frac{d^2\sigma}{d\Omega_c dE_c} = \frac{-2\rho(E_c)}{\hbar v_a} \int d\mathbf{r}_b \langle \Psi_0 | \chi_c^{(-)} \rangle(\mathbf{r}_b) \langle \chi_c^{(-)} | \Psi_0 \rangle(\mathbf{r}_b) \quad (75)$$

The partial overlap $\langle \chi_c^{(-)} | \Psi_0 \rangle$ is a source function for the removed particle, b . We call this source function $\rho_{\mathbf{k}_c}^{(+)}(\mathbf{r}_b)$.

If the three-body wave function Ψ_0 is replaced by $\chi_b^{(+)} \chi_c^{(+)} \phi_a$ (distorted wave approximation), we get the Hussein-McVoy (HM) source function $\rho_{\mathbf{k}_c}^{(HM)}(\mathbf{r}_b) \equiv \langle \chi_c^{(-)} | \chi_c^{(+)} \chi_b^{(+)} \phi_a \rangle$ and the corresponding HM expression for the inelastic break up cross-section

$$\begin{aligned} \frac{d^2\sigma_{ine.bup}}{d\Omega_c dE_c} &= \frac{-2\rho(E_o)}{\hbar v_a} \langle \rho_{\mathbf{k}_c}^{(HM)}(r_b) | W_b(r_b) | \rho_{\mathbf{k}_c}^{(HM)} \rangle \\ &= \frac{-2k_c \mu_c}{(2\pi)^3 \hbar^3 v_a} \langle \phi_a \chi_b^{(+)} \chi_c^{(+)} | \chi_c^{(-)} | W_b | \chi_c^{(-)} \chi_c^{(+)} \chi_b^{(+)} \phi_a \rangle \\ &= \frac{+2k_c \mu_c}{(2\pi)^3 \hbar^3 v_a} \langle \phi_a | \left(\left| \langle \chi_c^{(-)} | \chi_c^{(+)} \rangle \right|^2 \langle \chi_b^{(+)} | -W_b | \chi_b^{(+)} \rangle \right) | \phi \rangle \end{aligned} \quad (76)$$

From the general form of the total reaction cross-section

$$\sigma_{reac}^{(b)} = \frac{k_b}{E_b} \langle \chi_b^{(+)} | W_b | \chi_b^{(+)} \rangle \quad (77)$$

where the energy available for the b -particle is $E - E_c + |\varepsilon_0|$, with ε_0 being the binding energy of $b + c$, we can, after identifying $\langle \chi_c^{(-)} | \chi_c^{(+)} \rangle$ with the elastic S-matrix of the observed particle, $S_{\mathbf{k}_c \mathbf{k}_c}$, write for (HM) cross-section

$$\frac{d^2\sigma^{(HM)}}{d\Omega_c dE_c} = \frac{2k_c \mu_c E_b}{(2\pi)^3 \hbar^3 v_a k_b} \langle \phi_a | |S_{\mathbf{k}_c \mathbf{k}_c}|^2 \sigma_{Reac}^{(b)} | \phi_a \rangle \quad (78)$$

The above expression is a precursor to the eikonal one given in the previous section. The Bonaccorso-Brink [41, 42, 43] model is a time-dependent version of the above.

8 Nuclear break-up reactions of halo nuclei

The cross sections for Coulomb dissociation of halo nuclei are remarkably large, up to several barns. However, reactions with light targets also show large cross sections and narrow momentum distributions. The first such case was the observation [1] of a narrow transverse momentum distribution of ${}^9\text{Li}$ fragments from the reaction of ${}^{11}\text{Li}$ on a carbon target.

Nuclear reactions at intermediate and high energies may conveniently be treated in the eikonal approximation, which is valid if the energy is high and the scattering angle small. The form known as Glauber theory has been widely used for calculating nucleon-nucleus and nucleus-nucleus reactions at high energies. At the same time the collision time is short, so that it becomes permissible to treat the evolution of the final states in the sudden approximation. The paper by Bertsch, Brown and Sagawa [14] and subsequent work [36, 47] has applied these techniques to halo interactions with light targets. From the eikonal model it also follows that the outgoing fragment's longitudinal momentum distribution reflects the momentum content of the wave function in the volume sampled by the projectile's interaction with the target [48, 49]. The cross sections and momentum distributions are thus very sensitive to the angular momentum and separation energy of the nucleon in the initial state.

In the following we use the notation of Tostevin [40]. It is assumed that the nucleon is described by a normalized single-particle wave function with quantum numbers (nlj) moving with respect to the core of remaining nucleons in state $c \equiv I^\pi$. Such configurations are written $|\phi_{JM}^c\rangle$, where J is the magnitude and M the projection of the projectile's ground-state total angular momentum, $\mathbf{J} = \mathbf{I} + \mathbf{j}$. In the most frequent type of experiment, in which only the heavy residue is detected and not the neutrons, the single-particle cross sections are a sum of two contributions. These are usually referred to as *elastic breakup* (*diffraction dissociation*) and *absorption* (*stripping*) [12], so that we have $\sigma_{sp} = \sigma_{sp}^{diff} + \sigma_{sp}^{str}$. In the former, the nucleon and the heavy residue emerge from the reaction with essentially beam velocity. In the latter, the nucleon is scattered inelastically. These two contributions are computed separately, as integrals over the projectile's center of mass impact parameter, using a simple generalization of Eqs. 54 and 55.

$$\sigma_{sp}^{diff} = \frac{1}{2J+1} \int d\mathbf{b} \left[\sum_M \langle \phi_{JM}^c | (1 - \mathcal{S}_c \mathcal{S}_n)^2 | \phi_{JM}^c \rangle - \sum_{M, M'} |\langle \phi_{JM'}^c | (1 - \mathcal{S}_c \mathcal{S}_n) | \phi_{JM}^c \rangle|^2 \right] \quad (79)$$

and

$$\sigma_{sp}^{str} = \frac{1}{2J+1} \int d\mathbf{b} \sum_M \langle \phi_{JM}^c | (1 - |\mathcal{S}_n|^2) |\mathcal{S}_c|^2 | \phi_{JM}^c \rangle. \quad (80)$$

Here the quantities \mathcal{S}_c and \mathcal{S}_n are the elastic S-matrices, or *profile functions* [50, 51], for the core-target and removed neutron-target systems, expressed as functions of their individual impact parameters. These are calculated using the optical limit of Glauber theory [53]. The neutron-core relative motion wave functions $|\phi_{JM}^c\rangle$ are usu-

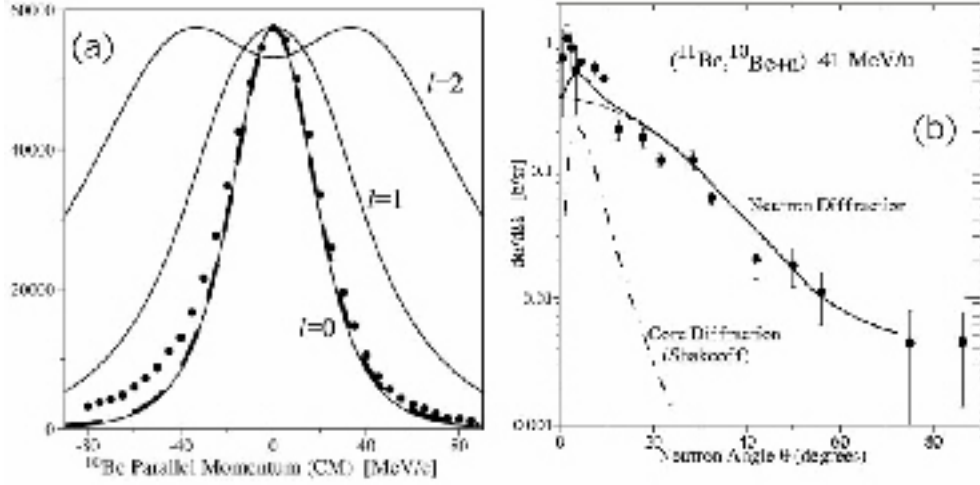


Figure 9 (a) The experimental longitudinal momentum distribution [21] for the ${}^9\text{Be}({}^{11}\text{Be}, {}^{10}\text{Be}_{gs})\text{X}$ reaction at an incident energy of 60 MeV/nucleon. The experimental data have been corrected for a 22% contribution from reactions leading to ${}^{10}\text{Be}$ excited levels. The errors are smaller than the point size. The full-drawn lines are calculations for $l=0,1,2$ in an eikonal approximation [21] and the heavy dashed line is the time-dependent treatment by Bonaccorso and Brink [41]. The calculations have been adjusted to the maximum height of the data (in arbitrary units). (b) Measured [54] exclusive angular distribution in the laboratory system of neutrons from the reaction ${}^9\text{Be}({}^{11}\text{Be}, {}^{10}\text{Be}+n)\text{X}$ at an incident energy of 41 MeV/nucleon. The theoretical total (full drawn line) is made up of three components. The main contribution arises from diffractive scattering of the neutron [41]. The excess at small angles is due to a combination [55] of shakeoff and Coulomb dissociation, which contribute a total of 16 mb. Inclusion of a finite-size correction (see [49]) would increase this by about 11 mb and would improve the agreement with experiment somewhat.

ally calculated in a Woods-Saxon potential with the depth of the potential adjusted to reproduce the separation energy of the nucleon. For high energies, for high l values, and for deeply bound states, the contribution from Eq. 80 is the largest, typically by a factor 2-3.

Equation 80 allows a simple interpretation. It is the integral over impact parameter and average over M substates of the joint probability of the core being left intact by the reaction (given by the quantity $|\mathcal{S}_c|^2$) and of the nucleon being absorbed (given by the quantity $(1 - |\mathcal{S}_n|^2)$). The diffractive cross section, Eq. 80, is derived within the HM theory, which use the spectator core plus nucleon model and employ closure to eliminate the necessary integral over all continuum final states of the dissociated core and nucleon [12]. The use of closure for obtaining the continuum contribution is clearly an excellent approximation for halos, where the ground state often is the only bound state.

Theoretical calculations of the longitudinal momentum distributions of the

core fragments may without significant loss of accuracy be made in a simpler model, based on the black-disc approximation [49, 50]. In this, \mathcal{S}_c and \mathcal{S}_n are assumed to be unity outside of a cutoff impact parameter and zero inside [21]. A good choice for core impact parameter cutoffs is to define them to reproduce core-target reaction cross sections [52], respectively the free-neutron reaction cross section (approximately 290 mb on a beryllium target at 60 MeV/nucleon). The widths of the momentum distributions are quite insensitive to the precise choice of the target radius and even the absolute cross sections agree well with more accurate approximations. As an example, Fig. 9(a) from the work of Aumann et al. [53] shows the longitudinal momentum distributions from the ${}^9\text{Be}({}^{11}\text{Be}, {}^{10}\text{Be}_{gs})X$ reaction. As we know today, the original experiment [9] that found the narrow distribution on a light target included a 22% contribution of reactions leading to excited states. This has been subtracted in the data of Fig. 9(a), which shows good agreement with the calculation assuming $l=0$ and definitely excludes $l=1,2$. There are small but distinct deviations, a slightly larger width and also an excess of events (a “tail”) on the low-momentum side. One believes that these effects arise in the diffractive channel. They are linked to energy conservation and can be accounted for in a fully quantum-mechanical calculation based on the discretised continuum coupled-channels method [56].

The results of Ref. [41, 42, 43] have also been applied to the longitudinal momentum distributions of neutrons from the breakup of halo states. They use a semi-classical (constant velocity, straight line) approximation for the relative motion of the core and target, with a lower impact parameter cutoff, but a (nonsudden) quantum-mechanical treatment of the interaction of the neutron with the target. The treatment deals with the diffractive and the stripping parts in a consistent way, and for the longitudinal momentum distribution shown in Fig. 9(b) it gives results that are very close to those obtained in the eikonal theory.

Only a few experiments have provided direct experimental evidence separating the diffractive breakup of the halo from the stripping reaction. This normally requires detection of the diffracted neutrons in coincidence with the charged residue. The characteristic signature [9] is a broad neutron angular distribution with an opening angle at half maximum of the order of $\theta_{1/2} = 1.6/(kR_T)$, where k is the neutron wave vector and R_T the target radius (see Supplement C). The result obtained by Anne et al. [52] for the case of ${}^{11}\text{Be}$, shown in Fig. 9(b), is in good agreement with this qualitative estimate. According to theory, the angular distribution of the neutrons has three contributions. The dominant one, calculated by Bonaccorso and Brink [41, 42, 43], is diffraction dissociation contributing 260 mb, in good agreement with the experimental value of 240 ± 50 mb. The excess of intensity at small angles is attributed [56] to Coulomb dissociation (9 mb) and to shakeoff (18 mb if a correction for the finite-size effect is included).

There is considerable experimental evidence showing the existence of proton halos. Reaction cross section data for ${}^8\text{B}$ indicate that it has a significantly extended wave function [57]. Smedberg et al. [55] have observed a narrow longitudinal momentum distribution for ${}^7\text{Be}$ fragments from proton removal from ${}^8\text{B}$. Similar results were found by Kelley et al. [58]. This is a particularly interesting case since the ${}^8\text{B}$

wave function has a strong influence on proton capture in the Sun, which is the source of the high energy neutrinos detected by most solar neutrino detectors on the Earth.

Much effort has been dedicated to the problem of the two-neutron halo, especially to the cases of ^{11}Li and ^6He . These are examples of three-body systems with the *Borromean property*, a term coined by Zhukov et al. [60] to denote systems for which the two-body sub-systems are unbound. The fact that, say, ^{11}Li is bound only through the combined effect of the $^9\text{Li}+n$ and the $n+n$ interactions led to the expectation that the central-field approximation will fail and that the wave function will show correlations reminiscent of the classic problem of the helium atom in atomic physics. The effects, indeed, turn out to be much more important in the nuclear case.

A central issue has been the angular-momentum components in the two-neutron wave function of ^{11}Li . Measurements of β -decay provided the first evidence for a mixed $s^2 + p^2$ structure.

Studies of the two-neutron halo by nuclear reactions were at first difficult because the direct experimental observables in Coulomb and nuclear reactions all are complicated by contributions from the reaction mechanism that we have only slowly learned to disentangle. An important step in this direction was done by Barranco et al. [37] showing how the transverse momentum distributions are influenced by diffractive and Coulomb effects and by final-state interactions. It is for these reasons that the longitudinal momentum distributions have come to play such an important role in the elucidation of the one-neutron halo, see Fig. 9(a). These are relatively free from diffractive and Coulomb effects and final-state interactions are absent or very small.

Simon et al. [61] suggest a new way of attacking the problem of the two-neutron halo. Basically, as applied to ^{11}Li , the idea is to reconstruct the combined momentum of the $^9\text{Li}+n$ residue in a stripping reaction on a light target. This directly relates to the momentum distribution of the stripped neutron in the same way as that of the core recoil from stripping of a single-neutron halo. The shape can only be fitted with a superposition of $s^2 + p^2$ components with about 50% of each. (For comparison, the p^2 contribution to the ground state of the helium atom is only 0.5%, see Slater [62]) An additional observable, not studied previously, is the relative phase between the components of the wave function. It was, for the first time, determined directly in the same experiment by observing the angular distribution of the decay products from the recoiling ^{10}Li . The strong forward-backward asymmetry demonstrates the interference of the $l=0,1$ final states in the single-neutron removal reaction. Similar experiments have been carried out for $^{6,8}\text{He}$ [63].

9 Spectroscopic information from break-up (knockout) reactions

It was pointed out early by Sagawa and Yazaki [64] that the observed inclusive momentum distribution of residues from the ($^{11}\text{Be}, ^{10}\text{Be}$) reaction on a light target will contain broad contributions from core knockouts leading to bound excited levels in ^{10}Be . For this it is necessary that the halo neutron will remain attached to the residue. Estimates show that the *shakeoff probability* is low (less than 10%).

The methods based on Glauber theory developed for halo states have a wider

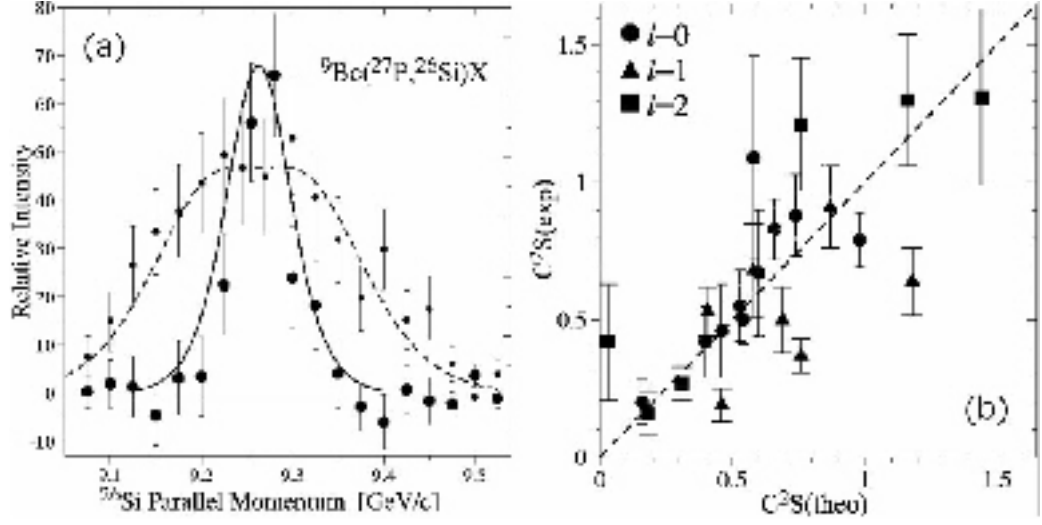


Figure 10 (a) Momentum distributions for the ${}^9\text{Be}({}^{27}\text{P}, {}^{26}\text{Si})\text{X}$ reaction to the ground state (large circles) and all excited states (small circles). The corresponding theoretical curves in arbitrary normalization are calculated in the eikonal theory. The full-drawn line corresponds to $l=0$ and the dashed one to $l=2$. (From [67]). (b) Comparison of experimental and calculated spectroscopic factors for reactions at approximately 60 MeV/nucleon leading to individual final levels in the nuclei ${}^{25,26,26}\text{Si}$, ${}^{10,11}\text{Be}$, ${}^{13}\text{B}$, and ${}^{14,15,16,18}\text{C}$ [67, 40, 53, 69]. Circles, triangles and squares correspond to $l=0,1,2$, respectively. The dashed line corresponds to $F=1$.

applicability. A number of experiments involving both halo and more bound “normal” states have been carried out. For the analysis of these experiments it is assumed [40] that the partial cross section $\sigma_{th}(I^\pi)$ for populating a given final state I^π of the residue can be written

$$\sigma_{th}(I^\pi) = \sum_j C^2S(I^\pi, nlj)\sigma_{sp}(S_n, nlj), \quad (81)$$

where C^2S is the spectroscopic factor for removal of a nucleon with given single-particle quantum numbers (nlj) . This quantity has been taken from many-body shell-model calculations by Brown and his collaborators [65, 66], and it expresses the parentage of the initial state with respect to a specific final state. The sum in Eq. 81 is taken over all configurations which have a nonvanishing parentage. The σ_{sp} are the single-particle removal cross sections, which are strongly dependent on the orbital angular momentum l and the nucleon separation energy S_n . The calculation of these quantities in an extension of Glauber theory has been discussed by Tostevin in [40, 54], and the basic expressions were given in equations 79 and 80.

As an example, we take a study of the proton-rich isotopes of phosphorus [67] which are interesting candidates for ground-state proton halos [69]. The isotopes ${}^{26,27,28}\text{P}$ are expected to have a dominant contribution of the $1s_{1/2}$ proton orbital,

and their proton separation energies of 0.14 ± 0.20 , 0.897 ± 0.035 and 2.066 ± 0.004 MeV, respectively, are low. The results [67] for the case of ^{27}P are shown in Fig. 10(a). The low counting statistics for the gamma spectrum made it necessary to resort to a gamma-ray tagging technique which divides the fragment data into two sets corresponding to coincidences and anti-coincidences with gamma rays. This requires knowledge of the average detection efficiency, $54 \pm 5\%$, estimated from the theoretical level scheme. The spectra also had evidence for a structureless continuum distribution with an intensity of $10 \pm 5\%$ above 0.25 MeV integral bias. This is attributed to neutrons, charged particles and γ rays produced in the target and to their secondary interactions with construction materials and the scintillator. (Later work [68, 69] has given more accurate estimates of this component but confirms the analysis in [67]. The measured gamma branching ratio of $30 \pm 10\%$ to the ground state corresponds to a partial cross section of 22 ± 8 mb, which translates into a $1s_{1/2}$ spectroscopic factor of 0.46 in excellent agreement with the theoretical spectroscopic factor obtained in the shell-model calculation. From the figure it is clear that the cross section to the ^{26}Si ground state is $l=0$ thus proving that the ground state of ^{27}P has spin and parity $1/2^+$. The figure also shows that the cross sections to the ^{26}Si excited levels are predominantly $l=2$ in agreement with theory. Similar results were found for other light phosphorus isotopes.

The results obtained by the knockout method are, so far, very promising. However, there is no reason to expect exact agreement between experiment and equation 81, which is a heuristic link between two unconnected theories. In order to test this relation experimentally, we define a scale factor F as the ratio between the experimental and the theoretical cross section. The scatter in F is then a test of the overall validity of this approach, while the average of F conveys information about possible empirical renormalizations. This would be analogous to the effective charges and effective coupling constants discussed for the sd shell by Brown and Wildenthal [65].

The nuclear-structure part of the theory has been eminently successful for nuclei up to mass 40, and we have much confidence in its predictions. Still, it is useful to recall that it is in some way a caricature of a real nucleus. It defines the spectroscopic factors in a severely truncated Hilbert space with nucleons assumed to be the fundamental building blocks. These are subject to effective interactions with strengths chosen to compensate for the neglected degrees of freedom. The reaction theory is less well proven experimentally. It starts from a picture of quasi-free nucleons, generally believed to be valid at considerably higher energies, and with key input parameters taken to be nucleon densities and (free) nucleon-nucleon scattering cross sections. Tostevin [40, 70, 54] has performed calculations based on other reaction models and has provided a substantial theoretical underpinning of the theoretical single-particle cross sections, which may be accurate to $\pm 20\%$. All results cited here are based on common, pre-existing parameter sets and individual adjustments have been avoided.

Two sets of data are, at the present time, available for comparisons. The experiments have measured l values and spectroscopic factors for 24 individual par-

tial cross sections for proton and neutron removal reactions in the p and sd shells. The comparison of experimental and theoretical spectroscopic factors given in Fig. 10(b) suggests an good overall agreement. Leaving out 5 cases with theoretical spectroscopic factors smaller than 0.4, one can calculate the average scale factor $\langle F \rangle$ separately for each l value. For the nine $l=0$ partial cross sections we obtain $\langle F_0 \rangle = 0.99 \pm 0.07$ with a χ^2 per degree of freedom of 1.1. Seven cases with $l=1$ give $\langle F_1 \rangle = 0.61 \pm 0.10$ where the (compound) experimental error has been scaled with the square root of the χ^2 per degree of freedom of 3.4. Finally, three $l=2$ partial cross sections give $\langle F_2 \rangle = 1.1 \pm 0.3$ with a χ^2 per degree of freedom of 1.6. The low value for $l=1$ may reflect contributions from high-lying $0^-, 1^-$ levels situated close to the neutron threshold in even-even nuclei.

At the present point in time, the majority of the data favor a scale factor close to unity. However, one expects to encounter major discrepancies in cases where the fundamental assumptions fail. This can happen if the dominant mechanism is not a direct reaction. The analysis of the ^{11}Be experiment [21] introduced small corrections for the competition from collective excitations caused by Coulomb and nuclear interactions. Two-step interactions must also play a role in certain reactions and small cross sections are, as always, suspect. There are also open experimental questions, especially for more deeply bound states, for which the cross section for diffraction dissociation, see Eq. 79, still needs to be tested experimentally. Nuclei nearer stability also have more complex spectra, and since the cross sections emerge from an input-output balance of γ -ray intensities, any substantial missed intensity can lead to systematic errors. Fortunately, this problem is smaller near the neutron drip line, where the nuclei have just a few bound levels. In the following we describe a theory for the angular distribution of inclusive break-up (stripping).

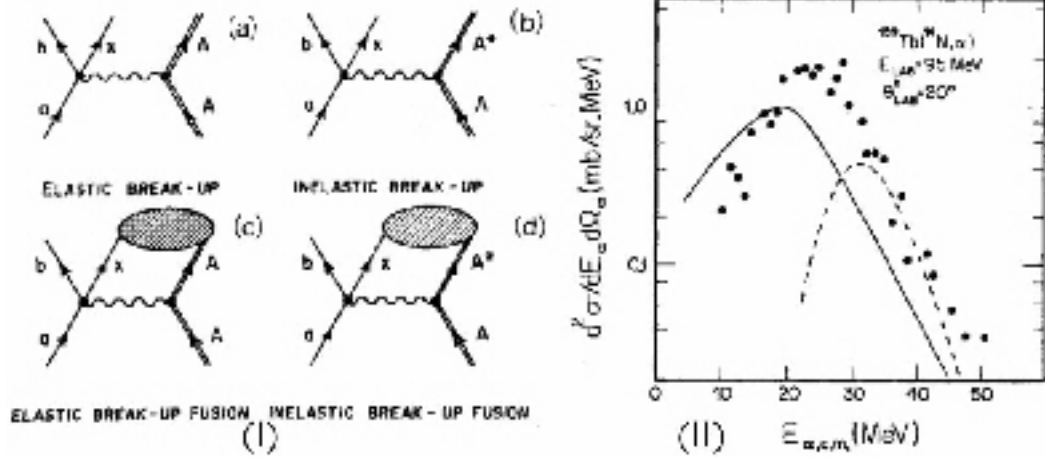


Figure 11 (I) Schematic diagrams representing the different processes that contribute to $d^2\sigma^{IB}/d\Omega_b dE_b$. (II) Calculated (full line) inclusive spectrum of α particles at $\theta = 20^\circ$ in the reaction $^{159}\text{Tb}(^{14}\text{N}, \alpha)$ at $E_{LAB} = 95$ MeV. The dashed curve is the result of the calculation of Ref. [45]. The data points were also taken from Ref. [45].

Supplement E

10 Angular distribution in inclusive break-up of halo nuclei

The cross section which describes a typical process

$$a + A \equiv (b + x) + A \rightarrow b + (x + A)^* \quad (82)$$

is written in the formalism of Hussein and McVoy [12, 71] as

$$\frac{d^2\sigma}{d\Omega_b dE_b} = \frac{2}{\hbar v_a} \rho(E_b) \left\langle \hat{\psi}_x^{(+)} | -W_{xA}(E_i + B_a - B_b) | \hat{\Psi}_x^{(+)} \right\rangle, \quad (83)$$

where $\rho(E_b)$ is the density of states of the b-particle, $\rho(E_b) = \mu_b k_b (2\pi)^3 \hbar^2 \cdot -W_{xA}$ is the imaginary part of the $x + A$ system and $\psi_x^{(+)}$ is the “negative energy” x -particle wave function [12, 71]

$$\hat{\psi}_x^{(+)}(\mathbf{r}_x) = \left\langle \chi_b^{(-)}(\mathbf{r}_b) | \varphi_a(\mathbf{r}_b - \mathbf{r}_x) \chi_a^{(+)}(\mathbf{r}_b, \mathbf{r}_x) \right\rangle, \quad (84)$$

where the χ 's are distorted waves and φ_a is the intrinsic wave function.

Using the notation of Ref. [12], we write the following general decomposition of the break-up cross section

$$\frac{d^2\sigma^{IB}}{d\Omega_b dE_b} = \frac{d^2\sigma_{dir}^{IB}}{d\Omega_b dE_b} + \frac{d^2\sigma_{fl}^{IB}}{d\Omega_b dE_b}, \quad (85)$$

the direct term describes what is called the *direct inelastic break-up* process while the *fluctuation part* accounts for incomplete fusion, the corresponding diagrams are shown in Fig. 11(I).

The expressions for the direct and the fluctuation components of $d^2\sigma^{IB}/d\Omega_b dE_b$ have been derived and discussed in Ref. [12]. The sum of the contributions of Fig. 11(I-a) (elastic break-up) and Fig. 11(I-b) inclusive (direct inelastic break-up) corresponds to the direct piece of the inclusive break-up cross section. Calling W_{xA}^{dir} the direct reaction part of W_{xA} , which accounts for the contribution of Fig. 11(I-b), we have for the direct component of the inclusive break-up cross section of Ref. [12]

$$\frac{d^2\sigma_{dir}^{IB}}{d\Omega_b dE_b} = \frac{2}{\hbar v_a} \left\langle \hat{\psi}_x^{(+)} \left| -W_{xA}^{dir}(E_i + B_a - B_b) \right| \hat{\psi}_x^{(+)} \right\rangle. \quad (86)$$

The difference, $W_{xA} = W_{xA}^{dir} \equiv w_{xA}^{fus}$, represents the fusion (compound nucleus) component of the absorptive piece of the xA optical potential. It appears in the expression for $d^2\sigma_{fl}^{IB}/d\Omega_b dE_b$ similarly to W_{xA}^{dir} in $d^2\sigma_{dir}^{IB}/d\Omega_b dE_b$, namely

$$\frac{d^2\sigma_{fl}^{IB}}{d\Omega_b dE_b} = \frac{2}{\hbar v_a} \left\langle \hat{\psi}_x^{(+)} \left| -W_{xA}^{fus}(E_i + B_a - B_b) \right| \hat{\psi}_x^{(+)} \right\rangle. \quad (87)$$

Eq. 87 represents the summed contribution of Figs. 11(I-c) and 11(I-d). Physically, it corresponds to the break-up of the projectile followed by the formation of the compound xA nucleus, both without (Fig. 11(I-c)) and with (Fig. 11(I-d)) concomitant inelastic excitation of the target nucleus.

At this point we remark that the numerical results obtained by Udagawa et al. [45], represent the contribution of diagram 11(I-c), namely elastic break-up fusion. We further remark that the principal result of Ref. [12] namely Eq. 83, represents a DWBA version of a more general expression for $d^2\sigma^{IB}/d\Omega_b dE_b$, derived in Ref. [44], in which the initial distorted product wave function is replaced by the exact Fadeev wave function of the interacting xbA system [44].

We next turn to more formal features of Eq. 87. We first rewrite this equation in the following form

$$\begin{aligned} \frac{d^2\sigma^{IB}}{d\Omega_b dE_b} &= \frac{2}{\hbar v_a} \rho(E_b) \left\langle \hat{\psi}_x^{(+)} \left| -W_{xA}(E_i + B_a - B_b) \right| \hat{\psi}_x^{(+)} \right\rangle \\ &\equiv \rho(E_b) \sigma_{reac}^{xA}(\Omega_b, E_b) \end{aligned} \quad (88)$$

where we have introduced, in the above, a new cross section which we call off-angle-and off-energy-shell total reaction cross section of the xA subsystem. We should stress that Eqs. 82, 83 and 84 do not contain the pure elastic break-up cross section.

The cross section that appears in Eq. 88 is related to the total xA reaction cross section when its angle variation is ignored and the system is allowed to be on the energy shell. In fact, this cross section does reduce to the usual reaction cross section times a Fermi-motion factor which contains the angle dependence when the distortion of the b particle (the spectator) and of the projectile is completely ignored. In this limit, one recovers the well known *Serber cross section* [12].

Since, here, the b -particle is allowed to optically scatter from the target (though without inflicting any non-elastic transition in the target), we have to discuss $\sigma_{react}^{xA}(\Omega_b, E_b)$ in all its generality, namely as an absorption cross section of a sub-system ($x + A$) which, accordingly, depends on the kinematical variable of the rest of the system (b). Several features of this cross section can be easily analyzed once the recognition is made that a very similar quantity to $\sigma_{react}^{xA}(\Omega_b, E_b)$, measures the deviation from unitarity of the two-body optical S -matrix [72].

In Ref. [72], the following equation was derived,

$$\langle \mathbf{k}' | S^{-1} | \mathbf{k} \rangle = \langle \mathbf{k}' | S^+ | \mathbf{k} \rangle + 2\pi\delta(E_{\mathbf{k}} - E_{\mathbf{k}'}) \int \frac{d\mathbf{k}''}{(2\pi)^3} \frac{2E_{\mathbf{k}''}}{k''} \langle \mathbf{k}' | S^{-1} | \mathbf{k}'' \rangle \sigma_{react}(\mathbf{k}, \mathbf{k}'') . \quad (89)$$

When $\sigma_{react}(\mathbf{k} \cdot \mathbf{k}'', |\mathbf{k}|, |\mathbf{k}''|)$ is set equal to zero one recovers the unitarity condition of the S -matrix “cross section” $\sigma_{react}(\mathbf{k} \cdot \mathbf{k}'', |\mathbf{k}|, |\mathbf{k}''|)$ becomes just the total reaction cross section $|\mathbf{k}| = |\mathbf{k}''|$ (which is the case in the above equation) and $\mathbf{k} \cdot \mathbf{k}'' = 1$.

The same quantity, $\sigma_{react}(\mathbf{k} \cdot \mathbf{k}'', |\mathbf{k}|, |\mathbf{k}''|)$ appears also in the equation which gives the orthonormality condition of the optical wave function $|\psi_k^{(+)}\rangle$,

$$\langle \psi_{k'}^{(+)} | \psi_k^{(+)} \rangle = (2\pi^3) \delta(\mathbf{k} - \mathbf{k}') - 2i \sqrt{\frac{E_{\mathbf{k}} E_{\mathbf{k}'}}{kk'}} \frac{\sigma_{react}(\mathbf{k}, \mathbf{k}')}{E_{\mathbf{k}} - E_{\mathbf{k}'} + i\epsilon\epsilon} , \quad (90)$$

When expanded in partial waves, $\sigma_{react}(\mathbf{k} \cdot \mathbf{k}'', |\mathbf{k}|, |\mathbf{k}''|)$ takes the following form

$$\sigma_{react}(\mathbf{k}, \mathbf{k}') = \frac{\pi}{kk'} \sum_{l=0}^{\infty} (2l+1) T_l(k, k') P_l(\hat{\mathbf{k}} \cdot \hat{\mathbf{k}}') , \quad (91)$$

where

$$T_l(k, k') = \frac{8\mu\sqrt{kk'}}{\hbar^2} \int_0^{\infty} dr \psi_l^*(k', r) W(r) \psi_l(k, r) . \quad (92)$$

$T_l(|\mathbf{k}|, |\mathbf{k}'|)$ on-the-energy shell ($|\mathbf{k}| = |\mathbf{k}'|$) becomes just the optical transmission coefficients, $T_l(|k|)$, which is related to the modulus of the optical partial wave S -amplitude,

$$T_l(|k|) = 1 - |S_l(k)|^2 . \quad (93)$$

On the energy-shell ($|\mathbf{k}| = |\mathbf{k}'|$), σ_{react} , becomes, in the sharp-cut-off limit ($T_l(|k|) = \Theta(l_g - l)$, where l_g is the grazing angular momentum)

$$\sigma_{react}(\mathbf{k}^2, \hat{\mathbf{k}} \cdot \hat{\mathbf{k}}') = \frac{\pi}{k^2} \left[P'_{l_g+1}(\hat{\mathbf{k}} \cdot \hat{\mathbf{k}}') + P'_{l_g}(\hat{\mathbf{k}} \cdot \hat{\mathbf{k}}') \right] , \quad (94)$$

where $P_l(x)$ is the Legendre polynomial and $P'_l(x) = dP_l(x)/dx$. Eq. 94 shows that σ_{react} exhibits oscillations as a function of $\hat{\mathbf{k}} \cdot \hat{\mathbf{k}}'$. These oscillations become more rapid as l_g increases.

We now turn to the effects arising from the dependence of σ_{react} on the off-shell variable $\xi \equiv |\mathbf{k}'| - |\mathbf{k}|$. To simplify the discussion we take ξ to be small enough that a Taylor series expansion of $\psi_l(k'r)$ can be contemplated. It is then clear that higher order terms in

ξ bring about terms in σ_{reac} which contain higher order Bessel functions. The alternating orders of these incoherently summed Bessel functions would thus bring about a damping of the θ -oscillations seen in the on-shell σ_{reac} . Then we may conclude that the larger ξ is the smooth $\sigma_{reac}(\theta)$ is expected. Similar features would be expected to be present in the inclusive break-up cross section $\sigma_{reac}^{xA}(\Omega_b, E_b)$, Eq. 88.

Now

$$\chi_k^{(+)}(\mathbf{r}) = e^{i\mathbf{k}\cdot\mathbf{r}} \exp\left(i \int_{-\infty}^z \Delta k(z', \mathbf{b}) dz'\right), \quad (95)$$

where $\Delta k(z', \mathbf{b})$ is given by

$$\Delta k(z', \mathbf{b}) = -\frac{k}{2E} U \Delta k(z', \mathbf{b}). \quad (96)$$

Here $U(z, \mathbf{b})$ is the complex optical potential. Using the above form for all wave functions appearing in Eq. 84, we obtain for $\psi_x^{(+)}$,

$$\begin{aligned} \hat{\psi}_x^{(+)}(\mathbf{r}_x, \mathbf{q}) &= e^{i\mathbf{k}_x \cdot \mathbf{r}_x} \exp\left(i \int_{-\infty}^{z_x} \Delta k_x(z', \mathbf{b}_x) dz'\right) \\ &\times \int d^3r_b e^{i\mathbf{q}\cdot\mathbf{r}_b} S'_{bA}(\mathbf{b}_b) \varphi_a(\mathbf{r}_b - \mathbf{r}_x). \end{aligned} \quad (97)$$

k_x is the relative momentum of the x -particle in the xA system, where $\mathbf{q} = \mathbf{k}_b - \mathbf{k}'_b$, the average momentum transfer from b to A by elastic scattering.

With the above form for $\psi_x^{(+)}$, we have for the inclusive cross section the following simple expression

$$\frac{d^2\sigma^{lR}}{d\Omega_b dE_b} = \rho(E_b) \sum_{l_x} P(q, l_x) \sigma_{reac}^{xA}(l_x), \quad (98)$$

$$P(q, l_x) = \frac{1}{2\pi} \int_0^{2\pi} d\phi |\hat{\varphi}_{a,b}(\mathbf{q}, l_x/k_x)|^2, \quad (99)$$

where $\varphi_{a,b}(\mathbf{q}, l_x/k_x)$ describes the zero-point relative motion (“Fermi motion”) of x and b within the projectile, which is broadened in the transverse direction by absorption of the spectator, namely

$$\hat{\varphi}_{a,b}(\mathbf{q}, \mathbf{b}_x) = e^{-iq_l z_x} \int d^3r_b e^{i\mathbf{q}\cdot\mathbf{r}_b} S_{bA}(\mathbf{b}_b) \varphi_a(\mathbf{r}_b - \mathbf{r}_x). \quad (100)$$

in Eq. 100 is the bA elastic scattering matrix. Finally σ_{reac}^{xA} is the l_x partial reaction cross section of the xA system.

We have evaluated Eq. 98 for the systems $^{158}\text{Tb}(^{14}\text{N}, \alpha)$ and $^{181}\text{Tb}(^{14}\text{N}, \alpha)$ at $E_{LAB} + 95$ MeV and 115 MeV, respectively. We have used for the real parts of the ba and xA optical potentials V_{bA} , V_{xA} , the double folding interaction [73] and merely multiplied these potentials by factors of the form $(1 + i\xi_{1b})$, respectively, where ξ_1 's are adjustable

imaginary strengths. As for the wave function $\phi_a(r)$, we used a Gaussian form, with a width σ , given by

$$\begin{aligned}\varphi_a(r) &= e^{-(\sigma^2/2)r^2}, \\ \sigma &= \frac{k_F}{\sqrt{5}} \sqrt{\frac{A_F(A_p - A_F)}{A_p - 1}},\end{aligned}\tag{101}$$

where A_F and A_p are the spectator (observed fragment) and projectile mass numbers, respectively, and k_F is the nuclear Fermi momentum of $\approx 1.36 \text{ fm}^{-1}$. For the system $^{159}\text{Tb} (^{14}\text{N}, \alpha)$ we get $\sigma = 2.1 \text{ fm}^{-1}$.

The result of such a calculation for the α -inclusive spectrum at 20° in $^{159}\text{Tb} (^{14}\text{N}, \alpha)$ at 95 MeV is shown in Fig. 11(II). The values of the parameter ξ_{1b} and ξ_{1x} are, respectively 0.01 and 0.5. The agreement with the data is quite good. Also shown are the results of Udagawa et al. [45] which greatly underestimate the cross section at the lower end of the spectrum. The reason is quite clearly the fact that Ref. [45] uses a model where only the elastic break-up fusion process, figure 11(I-c), is considered and in this order, whereas we include all processes shown in Fig. 11(I). Loosely speaking, the function $\psi_x^{(+)}$ of Udagawa contains an xA elastic propagator $G_x^{(+)}(E_x)$ which clearly damps the cross section at low E_b 's (high E_x) as it behaves, roughly, like E_x^{-1} . Incidentally, the total reaction cross section of the participant-target system, $^{10}\text{B} + ^{159}\text{Tb}$, extracted from this calculation, comes out within 20% of that extracted from the data of similar systems. This is reasonable in view of the usually large size of the error bars in σ_R .

Of course, we do not expect that this model to work as well at larger angles because of the Glauber approximation which is valid for small deflection angles. In fact, the angular distribution one obtains, has a much steeper slope than the data. Similar results were obtained for the angular distribution of the α , s from the $^{181}\text{Ta} (^{14}\text{N}, \alpha)$ reaction at $E_{LAB} = 112 \text{ MeV}$, Ref. [45].

11 References

1. T. Kobayashi et al., Phys. Rev. Lett. **60** (1988) 2599; T. Kobayashi, I. Tanihata, Proc. Int. Symposium on Structure and Reactions of Unstable Nuclei, June 17-19, 1991, Niigata, Japan, World Scientific, ed. by T. Suzuki.
2. I. Tanihata, on "Treatise on Heavy-Ion Science", Vol. 8, Ed. by D. Allan Bromley, (Plenum Publ., 1989).
3. A.S. Goldhaber, Phys. Lett. **B53** (1974) 306.
4. D.E. Greiner, P.J. Lindstrom, H.H. Heckman, B. Cork and F.S. Bieser, Phys. Rev. Lett. **35** (1975) 152.
5. G.F. Bertsch, Phys. Rev. Lett. **46** (1981) 472.
6. N. Orr, N. Anantaraman, S.M. Austin, C.A. Bertulani, K. Hanold, J.H. Kelley, D.J. Morrissey, B.M. Sherrill, G.A. Souliotis, M. Thoenessen, J.S. Winfield and J. Winger, Phys. Rev. Lett. **69** (1992) 2050.
7. C.A. Bertulani and K.W. McVoy, Phys. Rev. **C46** (1992) 2638.

8. Y.P. Viyogi, T.J.M. Symons, P. Doll, D.E. Greiner, H.H. Heckman, D.L. Hendrie, P.J. Lindstrom, J. Mahoney, D.K. Scott, K. Van Bibber, G.D. Westfall, H. Wieman, H.J. Crawford, C. McParland and C.K. Gelbke, *Phys. Rev. Lett.* **42** (1979) 33.
9. R. Anne, S.E. Arnell, R. Bimbot, H. Emling, D. Guillemaud-Mueller, P.G. Hansen, L. Johannsen, B. Jonson, M. Lewitowicz, S. Mattsson, A.C. Mueller, R. Neugart, G. Nyman, F. Pougheon, A. Richter, K. Riisager, M.G. Saint-Laurent, G. Schrieder, O. Sorlin and K. Wilhelmsen, *Phys. Lett.* **B250** (1990) 19.
10. D. Sackett, K. Ieki, A. Galonsky, C.A. Bertulani, H. Esbensen, J.J. Kruse, W.G. Lynch, D.J. Morrissey, N.A. Orr, B.M. Sherrill, H. Schultz, A. Sustich, J.A. Winger, F. Deák, Á. Horváth, Á. Kiss, Z. Seres, J.J. Kolata, R.E. Warner and D.L. Humphrey, *Phys. Lett.* **B300** (1993) 205; *Phys. Rev.* **C48** (1993) 118.
11. C.A. Bertulani and K.W. McVoy, *Phys. Rev.* **C48** (1993) 2534.
12. M. S. Hussein and K. W. McVoy, *Nucl. Phys.* **A445** (1985) 124.
13. M.S. Hussein, R.A. Rego, and C.A. Bertulani, *Phys. Reports* **201** (1991) 279.
14. G.P. Bertsch, B.A. Brown and H. Sagawa, *Phys. Rev.* **C39** (1989) 1154.
15. Y. Suzuki, *Nucl. Phys.* **A528** (1991) 395.
16. R. Serber, *Phys. Rev.* **72** (1947) 1008; *Annu. Rev. Nucl. Part. Sci.* **44** (1994) 1.
17. H. Utsunomiya, *Phys. Rev.* **C41** (1990) 1309.
18. C.A. Bertulani and G. Baur, *Phys. Rep.* **163** (1988) 299..
19. M.V. Zhukov *et al.*, *Nucl. Phys.* **A529** (1991) 53; *Nucl. Phys.* **A539** (1992) 177.
20. P.G. Hansen, *Phys. Rev. Lett.* **77** (1996) 1016.
21. J. H. Kelley et al., *Phys. Rev. Lett.* **74** (1995) 30.
22. W. Schwab et al., *Z. Phys.* **A350** (1995) 283.
23. B. A. Brown, A. Csótó and R. Sherr, *Nucl. Phys.* **A597** (1996) 66.
24. H. Sagawa, B. A. Brown, and H. Esbensen, *Phys. Lett.* **B309** (1993) 1; T. Otsuka, N. Fukunishi, and H. Sagawa, *Phys. Rev. Lett.* **70** (1993) 1385.
25. A. Csótó, *Phys. Lett.* **B315** (1993) 24.
26. I. Tanihata, *Prog. Part. Nucl. Phys.* **35** (1995) 505.
27. K. Gottfried, *Quantum Mechanics* (Benjamin, New York, 1966), Vol. I, p. 114.
28. R. Anne et al., *Nucl. Phys.* **A575** (1994) 125; *Phys. Lett.* **B304** (1993) 55.
29. I.S. Gradshteyn and I.M. Ryzik, “*Table of integrals, series and products*”, Academic Press, NY, 1965.
30. P.G. Hansen, A.S. Hansen and B. Jonson, *Ann. Rev. Nucl. Part. Sci.* **45** (1995) 591.
31. R. W. Finlay et al., *Phys. Rev.* **C47** (1993) 237; W. Schimmerling et al., *Phys. Rev.* **C7** (1973) 248; J. Franz et al., *Nucl. Phys.* **A490** (1988) 667; G. J. Igo et al., *Nucl. Phys.* **B3** (1967) 181.
32. I. Pecina et al., *Phys. Rev.* **C52** (1995) 191.
33. H. Esbensen, *Phys. Rev.* **C53** (1996) 2007.
34. A.I. Akhiezer and A.G. Sitenko, *Phys. Rev.* **106** (1957) 1236.
35. See, e.g. P.G. Hansen and M.B. Sherrill, *Nucl. Phys.* **A693** (2001) 133.
36. K. Yabana, Y. Ogawa, and Y. Suzuki, *Nucl. Phys.* **A539** (1992) 293.
37. F. Barranco, E. Vigezzi and R.A. Broglia, *Phys. Lett.* **B319** (1993) 387.
38. H. Esbensen, *Phys. Rev.* **C53** (1996) 2007.

39. G.F. Bertsch, K. Hencken and H. Esbensen, Phys. Rev. **C57** (1998) 1366.
40. J.A. Tostevin, J. Phys. **G25** (1999) 735.
41. A. Bonaccorso and D.M. Brink, Phys. Rev. **C57** (1998) R22.
42. A. Bonaccorso and D.M. Brink, Phys. Rev. **C58** (1998) 2864.
43. A. Bonaccorso, Phys. Rev. **C60** (1999) 054604.
44. N. Austern *et al.*, Phys. Reports **154** (1987) 125.
45. T. Udagawa, X.-H. Li and T. Tamura, Phys. Lett. **B143** (1984); T. Udagawa, Invited talk given at Int. Workshop on *Coincident particle emission from continuum states*, Bad Honnef, W. Germany, June 4-7, 1984.
46. G. Baur, F. Rosel, D. Trautmann and R. Shyam, Phys. Reports **111** (1984) 333.
47. G.F. Bertsch, H. Esbensen, and A. Sustich, Phys. Rev. **C42** (1990) 758.
48. J.S. Al-Khalili, J.A. Tostevin, and I.J. Thompson, Phys. Rev. **C 54** (1996) 1843.
49. J.A. Tostevin and J.S. Al-Khalili, Nucl. Phys. **A616** (1997) 418c.
50. R.J. Glauber, in *Lectures in Theoretical Physics*, edited by W.E. Brittin (Interscience), 1959.
51. S. Kox *et al.*, Phys. Rev. **C35** (1987) 1678.
52. R. Anne *et al.*, Phys. Lett. **B304** (1993) 55; Nucl. Phys. **A575** (1994) 125.
53. T. Aumann *et al.*, Phys. Rev. Lett. **84** (2000) 35.
54. J. Tostevin, Nucl. Phys. **A682** (2001) 320c.
55. M.H. Smedberg *et al.*, Phys. Lett. **B452** (1999) 1.
56. F. Barranco and P.G. Hansen, Eur. Phys. J. **A7** (2000) 179.
57. R.E. Warner *et al.*, Phys. Rev. **C52** (1995) R1166.
58. J.H. Kelley *et al.*, Phys. Rev. Lett. **77** (1996) 5020.
59. A. Kasano and M. Ichimura, Phys. Lett. **B115** (1982) 81; M. Ichimura, N. Austern and M. Vicent, Phys. Rev. **C32** (1985) 431.
60. M.V. Zhukov *et al.*, Phys. Rep. **231** (1993) 151.
61. H. Simon *et al.*, Phys. Rev. Lett. **83** (1999) 496.
62. J.C. Slater, *The Quantum Theory of Matter* (McGraw-Hill 1968) p. 442.
63. K. Markenroth *et al.*, Nucl. Phys. **A679** (2001) 462.
64. H. Sagawa and K. Yazaki, Phys. Lett. **B244** (1990) 149.
65. B.A. Brown, B.H. Wildenthal, Ann. Rev. Nucl. Part. Sci. **38** (1988) 29.
66. E.K. Warburton and B.A. Brown, Phys. Rev. **C46**, 923 (1992).
67. A. Navin *et al.*, Phys. Rev. Lett. **81** (1998) 5089.
68. A. Navin *et al.*, Phys. Rev. Lett. **85** (2000) 266.
69. V. Maddalena *et al.*, Phys. Rev. **C63** (2001) 024613.
70. J.A. Tostevin, in *Fission and Properties of Neutron-rich Nuclei*, Proceedings of the Second International Conference, St Andrews, Scotland, 28 June - 3 July 1999, edited by J.H. Hamilton, W.R. Phillips, and H.K. Carter (World Scientific, Singapore, March 2000), p. 429.
71. M.S. Hussein, Ann. of Phys. **175** (1987) 197; **11** (1987) 58.
72. W.A. Friedman, Phys. Rev. **C27** (1983) 569.
73. A. Budzanowski, G. Gaur, C. Alderliesten, J. Bojowald, C. Mayer-Böricke, W. Oelert,

- P. Turek, F. Rösel and D. Tratmann, Phys. Rev. Lett. **41** (1978) 635.
74. F.D. Becchetti Jr. and G.W. Greenless, Phys. Rev. **182** (1969) 1190.